Elasto Plastic Analysis of the Peel Test

by

Kyung-Suk Kim
Department of Theoretical and Applied Mechanics
University of Illinois at Urbana-Champaign
Urbana, Illinois 61801

February 28, 1985

Project Number: IBM PEEL TEST (441614)

Contents

I. Abstract

In the first year (1984) study of this project (Project #: IBM Peel Test, UI account #1-5-37119), an analytic method has been developed to analyze the elasto-plastic deformation of thin films in peeling process. With the analytic method, we could extract the adhesion bond energy from the peel-test values of thin (1 μm ~ 1 mm) metallic films. The validity of the analysis was verified by numerical and experimental analysis. The experimental analysis has been carried out by Dr. J. I. Kim of IBM independently. These studies extended the applicability of peel test from elastic peeling to elasto-plastic peeling. In particular, the analytic result strongly supports the validity of peel test with large amount of ductility (plasticity) that is inevitable in peel test of thin metallic films with strong adhesion. In particular, universal peel diagram is invented in this study. On the single universal peel diagram, interrelations of peel strength and adhesion energy can be readily read for all combinations of the material properties and the geometry (thickness of the adherend) of the specimen. In addition, the peel strength can be easily converted to pull strength using this diagram. The theory and the analytic results agree excellently with experimental results. (The experimental information was provided by Drs. L. Lee, P. Geldermans and J. Kim of IBM.)

II. Introduction

The peel test has long been used to characterize the strength of adhesion [1-5]. However, recent studies showed that the peel strength is a direct measure of adhesion energy only under a condition [6,7]. The condition is $6EP/\sigma_y^2 < t$, where E, σ_y, t are elastic (Young's) modulus, yield stress, thickness of the adherend and P is the measured peel strength. This condition is too strong to be satisfied for practical peel test of thin film adhesion in computer industries. For example, the thickness of copper adherend has to be in the order of 1 cm or more to satisfy the condition with typical adhesion strength of modern products. On the other hand, the thickness of the adherend of interest is in the order of $0.1 \sim 1000$ μm. This is the reason why we initiated this project last year to extend the applicability of peel test to practical range of adherend-thickness and adhesion-strength.

In this report; a new analytic method has been developed to extract the adhesion energy from the peel strength of a very thin metallic film (down to 10 μm thickness with strong adhesion). The analytic method allows plastic deformation of the adherend. With this analytic method, various aspects of peeling process in practical peel test have been investigated. The analysis includes theoretical formulations and solution methods, finite element method (FEM) analysis. These analyses are supported by experimental investigations carried out independently by Dr. J. I. Kim at IBM. These analyses extended the applicability of peel test to the range of $\frac{P}{\sigma_y \varepsilon_f} < t \leq \frac{6EP}{\sigma_y^2}$. Here ε_f indicates failure strain (ductility of the adherend, e.g., ε_f 0.55 for pure copper). The new adherend-thickness range spans $1\ \mu m < t < 1$ cm for copper adherend with usual adhesion strength. This range covers most of the adherend-thickness currently employed for packaging in computer industries.

When the thickness is less than $P/\sigma_y\varepsilon_f$, peel test can not be made because the adherend itself breaks. For the test of such an ultra-thin adherend, a new experimental method has to be developed.

With the analytic method, the framework of the analysis of elasto-plastic peeling has been completed. The theoretical formulations and the corresponding solutions are obtained for elastic-perfect plastic, elastic-linear harnening, elastic-2 parameter power-law-hardening models of the adherend. In addition, kinematic-hardening [8] and isotropic-hardening [9] rules are employed for the change of yield surfaces. The 2 parameter power-law hardening can give fairly accurate description of stress-strain relation of copper up to 30% plastic strain. The analysis shows the roles of the properties of adherend, e.g., elastic modulus, yield stress, hardening parameters, thickness, etc., in extracting the adhesion energy from the peel strength. Also, it is found that the elastic property of the substrate plays important role for the determination of adhesion energy.

The theoretical analysis carried out in the first year period covers two stages (the first and third) among the three stages of peeling process. The first stage is the deformation process up to onset of peel propagation: the second stage is the transient state of peel propagation: the third stage is the steady state peel propagation. In this analysis it is found that there are four different states of deformation pattern in the first stage, depending on the strength of adhesion for a given thickness of the adherend. The four states include elastic-bending, elasto-plastic-bending, unloading-and-localized-active-bending, reverse-plastic-bending states just prior to peel propagation. These initial states determine the subsequent drop or increase of peel force at the initiation of peel propagation. For the third stage, Dr. J. I. Kim found, experimentally, that the frequency and amplitude of peel-

force fluctuation is a function of adherend thickness. The fluctuation is caused by stick-slip behavior of peel propagation. The stick-slip behavior becomes more significant for thinner adherends. The stick-slip peel propagation is believed to be one of the key mechanisms of debonding process for very thin metallic films. Therefore, it is worth studying in more detail.

The theoretical study could predict the profile of the adherend and peel-force-stroke curve. The prediction was made for the first three deformation states of the first stage, and for the third stage of the peel process. These analytic results have been favorably compared with numerical and experimental results. The numerical results gave details of the stress distribution in both adherend and substrate. The numerical analysis was also able to check the practical local-debonding criteria, such as critical crack opening displacement (COD) [10], critical strain energy density [11], etc., in the second (transient) stage of peel propagation. It is found that the transient behavior of peel propagation is very sensitive to choice of debonding criteria. Therefore it is believed that the detail study of transient stage of peel propagation would provide practical local-debonding-criteria. In addition, the inter-relation between pull stress and peel force has been investigated. Details of all the analytic results are reported in Chapter IX.

In addition to the detail analysis, as a summary, a universal peel diagram (pt diagram) is proposed. The diagram has been constructed for copper adherend on silicon and polyimide substrates. From this diagram, the adhesion energy, γ , can be readily read, knowing the peel force, p , and thickness, t . (If you know any two of $[p,t,\gamma]$, then you can read the other value from the diagram.) This diagram is extremely valuable, not only for the engineers and designers, but also for the physicists and chemists. For the engineers, this diagram paves the way to predict (or prevent) other modes of

failure with the peel test. Knowing the adhesion energy, γ , designers can choose proper thickness for an expected peel value. The scientists can tell the state of interfacial bonding from the peel test values using this diagram. Also the method of constructing this diagram with experimental tests is provided in this report.

III. Energy Balance in Peeling

Peel test has been widely used to characterize the adhesion of a thin layer attached to a substrate. The major advantage of peel test is that experiment is relatively simple and that the peel strength and the interfacial bond strength have a conceptually simple relationship. The conceptually simple reltionship is the energy balance in peeling. In general a part of the work done by the peel force is used to break the interfacial bonding. The other part of the work is, in part, dissipated in the form of heat through plastic deformation and the rest is stored as elastic strain energy of the residual stress.

For an elastic peeling, the plastic work dissipation is excluded. The mechanism (plasticity) of producing residual stress is also excluded. Therefore all the work done by the peel force is used to create the interfacial fracture surface. This is true if the configuration (shape) of the adherend and the substrate does not change near the interfacial crack tip. This condition can be satisfied if the length-wise dimension of the specimen is much greater than the thickness of the adherend. Suppose that the conditions are satisfied to have perfect elastic peeling. Then, as shown in Fig. III-1, the interfacial fracture energy per unit area, Γ_o, can be expressed as

$$\Gamma_o = F\, d\ell/wd\ell = F/w = p. \qquad \text{(III-1)}$$

Here, F is the total peeling force and w is the width of the adherend and $d\ell$ is the virtual advance of the peel-crack. p is defined as the peel force (per unit width). The interfacial fracture energy, Γ_o, can be considered as atomic bond energy x number of atomic bonding per unit area. Eqn. III-1 tells

us that the peel force itself is the measure of the interfacial fracture (surface) energy.

In order to see details of how the energy is expended for peel propagation, consider the J integral [12] along a contour Γ around the crack tip as shown in Fig. III-2. The J integral is defined as

$$J = \int_{\Gamma} (\Phi\, n_1 - \underline{T} \cdot \frac{\partial \underline{u}}{\partial x_1}) \, ds \qquad \text{(III-2)}$$

where Φ is the strain energy density per unit undeformed configurational volume and n_1 is the x_1 component of the normal vector $\underline{n}$ to the contour Γ and $\underline{T}$ is the nominal traction vector (inner product of 1st Piola-Kirchhoff stress and $\underline{n}$) and $\underline{u}$ is the displacement and s is the arc length along the contour Γ. For this type of configuration, J is path independent if the material remains to be elastic everywhere. Also J is identical to energy release rate (energy expenditure per unit advance of the crack tip) in this case. If we take Γ along the boundary of the specimen, that is far away from the crack tip, J becomes

$$J_{far} = P + P^2/(2Et). \qquad \text{(III-3)}$$

However, in general, $p >> p^2/(2Et)$ so that $J_{far} \cong P$. On the other hand if we take Γ just around the crack tip, then J becomes

$$J_{near} = \int_{b}^{\delta_t} \sigma_{bs} \, d\delta = \bar{\sigma}_{bs} \, \delta_t. \qquad \text{(III-4)}$$

Here δ_t is the crack tip opening displacement and b is the unstretched atomic distance, and σ_{bs} is the interfacial bonding stress (interatomic force x number of atoms per unit area). $\bar{\sigma}_{bs}$ is an average bond stress. Then, because the J integral is path independent, J_{far} is equal to J_{near} and consequently from eqs. (III-3) and (III-4),

$$P \tilde{=} \bar{\sigma}_{bs} \delta_t . \qquad \text{(III-5)}$$

In Fig. III-3, two possibilities of the configuration of debonding process zone are shown. Those are the cohesive and interfacial debonding. For cohesive debonding, the peel force, p, is a lower bound of the intefacial bonding energy per unit area. In this case, peel force is the measure of the fracture energy of either substrate or adherend.

If plastic deformation undergoes with peeling, we have to account for the plastic work rate in the energy balance relation. However it is somewhat complicated to estimate the plastic work rate. The plastic work rate becomes important when $\eta (= 6EP/\sigma_y^2 t)$ is greater than unity, in 90° peel test. The plastic deformation is considered to be contributed by two major sources. One is the plastic deformation caused by near tip stress (or strain) concentration. The other is the plastic deformation caused by bending mode of the adherend. For most of thin film peeling, however, the plastic work rate due to the bending mode is predominant. Throughout this report, the plastic work rate of bending mode is considered as the only energy-dissipation source. In this approximation, the difference between the actual work rate of the adherend and the work rate of bending mode is considered to be very small comparing to the actual work rate. Then,

$$p = \gamma + \phi \left(\ell_R \right) \qquad \text{(III-6)}$$

where ϕ is the work expenditure rate, per unit advance of the peel propagation, caused by the plastic deformation in the adherend and γ is the adhesion energy; substate is assumed to remain elastic. The work expenditure rate ϕ is composed of two parts,

$$\phi = \frac{dW^P}{d\ell} + \frac{d\Phi}{d\ell} \qquad \text{(III-7)}$$

where $\frac{dW^P}{d\ell}$ is the plastic work dissipation rate per unit advance of peeling, in local continuum sense, and $\frac{d\Phi}{d\ell}$ is the residual-strain energy production rate per unit advance of peeling. In this report, this energy balance concept is used to develop the convenient universal peel diagram.

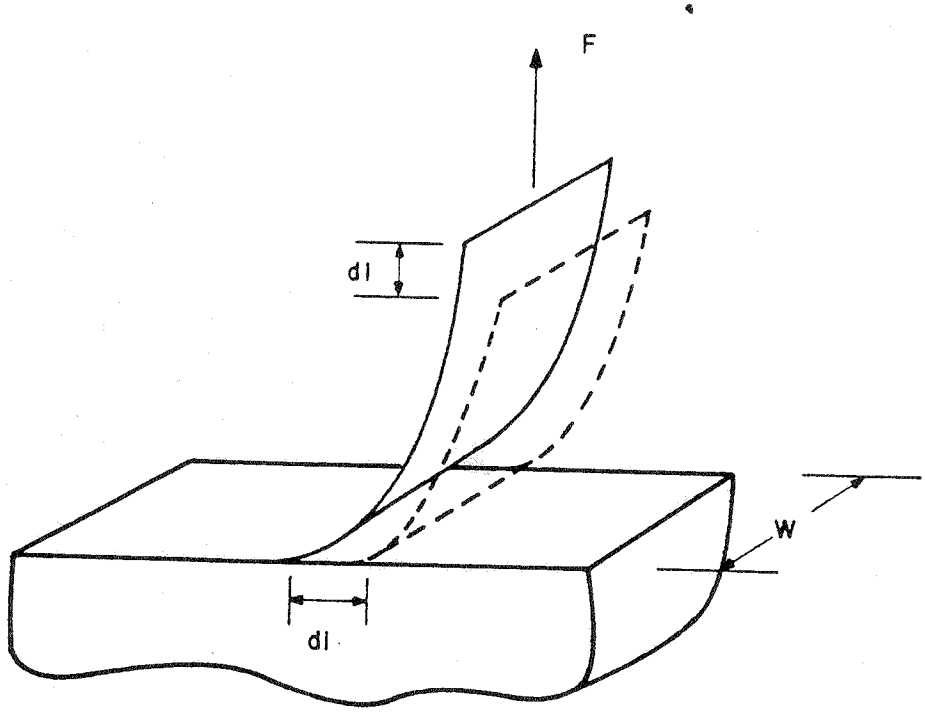

Fig. III-1

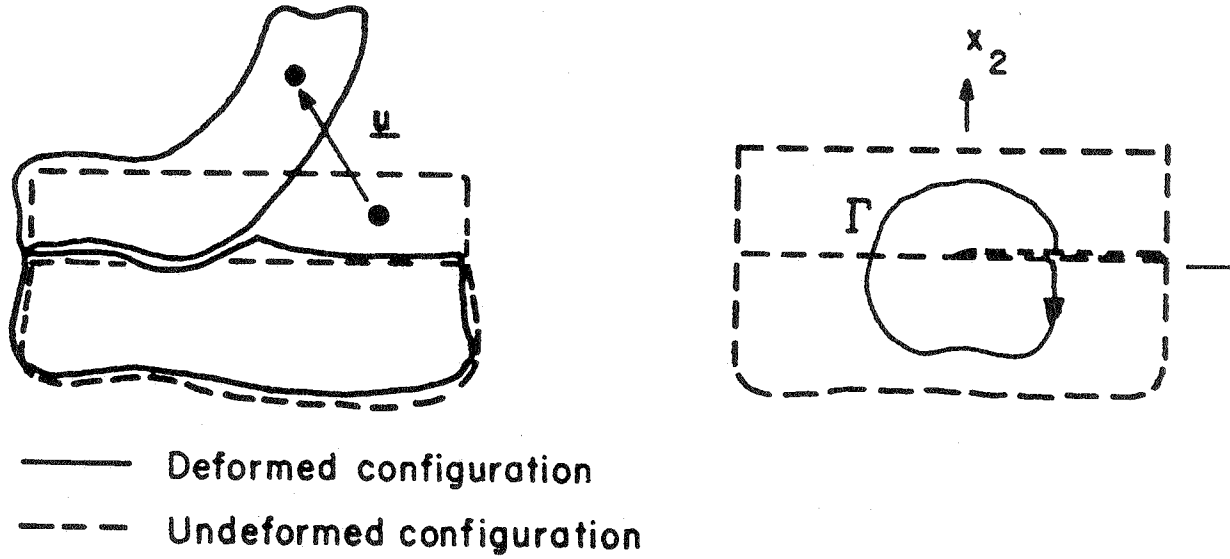

Fig. III-2

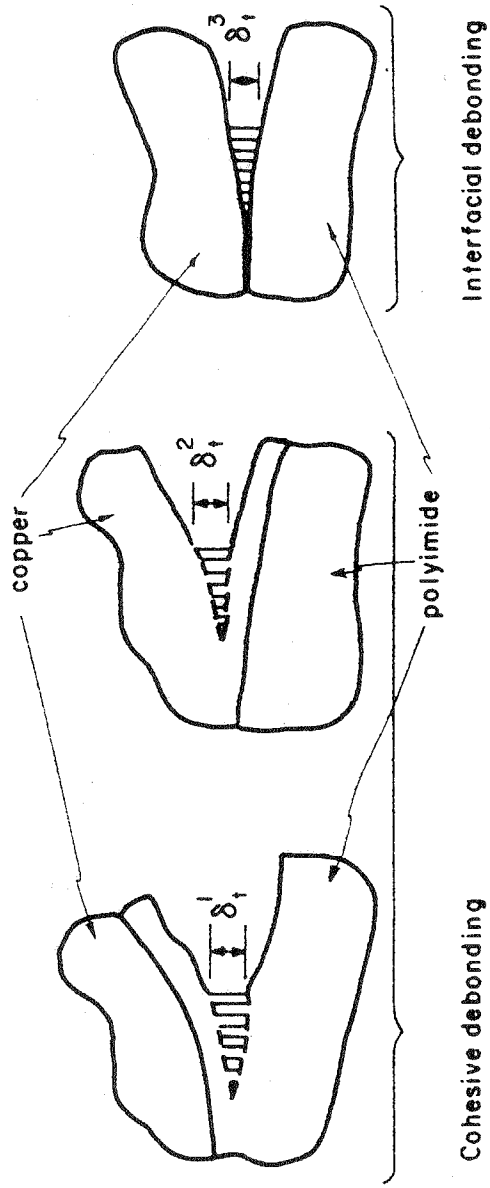
δ_t^3
δ_t^2
δ_t^1
copper
polyimide
Interfacial debonding
Cohesive debonding

Fig. III-3

IV. Analysis Up to Onset of Peeling

A. Governing Equations of Adherend Deformation

As mentioned in the previous chapter, we assume that the bending is the predominant deformation mode of the adherend. Therefore we extend the one-dimensional slender beam theory [13] to the deformation of general elasto-plastic adherend. This may be called "plastica problem".

Consider the deformed configuration of the adherend as shown in Fig. IV-1. Let u and v be the local coordinate composed of tangential and normal directions. Then the local equilibrium (force balance) in u and v direction gives the equilibrium equations as,

$$\frac{dT}{ds} - K N = 0 \qquad \text{(IV-1)}$$

$$\frac{dN}{ds} + K T = 0 \qquad \text{(IV-2)}$$

where T is the tensile force (per unit width) along the adherend, N is the shar force normal to the adherend and s is the arc length along the adherend. K indicates the local curvature defined by $K = \frac{d\theta}{ds}$, where θ is the angle between the tangential line to the adherend and the horizontal base line. Besides these two force-balance equilibrium equations, there is a moment-balance equilibrium equation,

$$\frac{dM}{ds} + N = 0 \qquad \text{(IV-3)}$$

where M is the bending moment of the adherend. Other than these 3 equilibrium equations, we need another equation for 4 unknowns, T,N,M, and K. It is the moment-curvature relation. In simple beam bending theory, we assume that the plane sections perpendicular to neutral axis remain to be planes and that the neutral axis coincide with central axis. The first assumption, turns

out to be a reasonable approximation even for the high curvature gradient along the adherend. This is verified later by finite element analysis in Chapter V. The second assumption is also a good approximation provided the final radius of curvature is not less than four or five times the thickness of the adherend. Throughout our study, the maximum curvature in peel test of copper adherend satisfies the condition. When the maximum curvature violates condition, the general theory of sheet bending (see Mathematical Theory of Plasticity by R. Hill [14]) has to be applied for the particular case. Then the assumption imposes that strain, $\varepsilon = - K v$ (see the geometry of bending in Fig. IV-2). The relation give the bending moment as

$$M = - \int_{-t/2}^{t/2} \sigma\{\varepsilon\} \, v \, dv = - \int_{-t/2}^{t/2} \sigma\{-Kv\} \, v \, dv \qquad \text{(IV-4)}$$

where $\sigma\{\varepsilon\}$ is the stress dependent upon the history of strain.

The constitutive relations, $\sigma[\varepsilon]$, used in our study are elastic-perfect plastic constitutive relation and parameter power law hardening constitutive relation. The schematic drawing of the relation is shown in Fig. (IV-3). σ_o in the figure indicates the flow stress. The bending moment-curvature relation is, then, obtained by Eqn. (IV-4). Normalizing the moment and curvature by ultimate limit bending moment, M_o , and elastic limit curvature, K_e, as

$$m = M/M_o; \qquad M_o = \sigma_o t^2/4 \qquad \text{(IV-5)}$$

$$k = K/K_e; \qquad K_e = 2\sigma_o/Et, \qquad \text{(IV-6)}$$

we get the following expressions (Also see reference [15] and Fig. (IV-4).

(a) elastic stage (O-A)

$$m = \frac{2}{3} k \; ; \qquad 0 \leq k \leq 1 \tag{IV-7}$$

(b) plastic loading stage (A-B)

$$m = 1 - \frac{1}{3k^2} \; ; \qquad 1 < k \leq k_B \tag{IV-8}$$

(c) elastic unloading stage (B-E)

$$m = \frac{1}{3} \left[3 - \left(\frac{1}{k_B^2} + 2 k_B\right) + 2k\right] \tag{IV-9}$$

(d) plastic reverse loading (E-I)

$$m = \frac{1}{3} \left[- 3 - \frac{1}{k_B^2} + \frac{8}{(k_B - k)^2}\right] \tag{IV-10}$$

(e) complete reverse plastic loading (I - - ∞)

$$m = - \left(1 - \frac{1}{3k^2}\right) \tag{IV-11}$$

Similarly, for a one-parameter power-law hardening material for which

$$\sigma = E \varepsilon \; ; \qquad \varepsilon < \varepsilon_y \tag{IV-12}$$

$$\frac{\sigma}{\sigma_y} = \left(\frac{\varepsilon}{\varepsilon_y}\right)^n \; ; \qquad \varepsilon \geq \varepsilon_y \; ; \qquad 0 \leq n \leq 1 \tag{IV-13}$$

we can get the moment-curvature relation. However in this case we have to use yield stress σ_y in place of flow stress σ_o for the normalization. ε_y indicates the yield strain. The bending moment-curvature relation is obtained as,

(A) elastic stage (0-A)

$$m = \frac{2}{3} k \; ; \qquad 0 \leq k \leq 1 \tag{IV-14}$$

(B) plastic loading stage (A-B)

$$m = \left(\frac{2}{3} - \frac{2}{n+2}\right) \frac{1}{k^2} + \frac{2}{n+2} k^n \; ; \quad 1 \leq k \leq k_B \tag{IV-15}$$

(C) elastic unloading stage (B-E)

$$m = \left(\frac{2}{3} - \frac{2}{n+2}\right) \frac{1}{k_B^2} + \frac{2}{n+2} k_B^n + \frac{2}{3} (k - k_B) \; ;$$

$$k_E < k < k_B \tag{IV-16}$$

here $k_E = k_B - 2$ for kinematic hardening and $k_E = k_B - 2\, k_B^n$ for isotropic hardening.

(D) plastic reverse loading (E-I)

$$m = \left(\frac{2}{3} - \frac{2}{n+2}\right) \frac{1}{k_B^2} - \frac{2}{n+2} k_B^n - 2k_B^n \left(\frac{2}{3} - \frac{2}{n+2}\right) \left(\frac{k_B - k}{2k_B^n}\right)^{\frac{n+2}{n-1}}$$

$$- k_B \leq k \leq k_B - 2 \text{ (kinematic hardening)} \tag{IV-17}$$

(E) complete reverse loading (I - - ∞)

$$m = - \left(\frac{2}{3} - \frac{2}{n+2}\right) \frac{1}{k^2} - \frac{2}{n+2} (-k)^n \; ; \quad k < - k_B \tag{IV-18}$$

However in many cases, the one-parameter hardening model can not fit the actual stress-strain relation in good approximation. Then we have to employ 2 parameter hardening model as

$$\sigma = E \varepsilon \; ; \quad \varepsilon < \varepsilon_y \tag{IV-19}$$

$$\frac{\sigma}{\sigma_y} = (1-s) \left(\frac{\varepsilon}{\varepsilon_y}\right)^n + s; \quad \varepsilon \geq \varepsilon_y, \tag{IV-20}$$

$$0 \leq n \leq 1,$$

$$0 \leq s \leq 1.$$

For this type of 2-parameter power hardening material we have the following

moment curvature relation.

(α) elastic loading (O-A)

$$m = \frac{2}{3} k \; ; \quad 0 \leq k \leq 1 \tag{IV-21}$$

(β) plastic loading (A-B)

$$m = \left(\frac{2}{3} - \frac{sn+2}{n+2}\right) \frac{1}{k^2} + \frac{2(1-s)}{n+2} k^n + s;$$

$$1 \leq k \leq k_B \tag{IV-22}$$

(γ) elastic unloading (B-E)

$$m = \left(\frac{2}{3} - \frac{sn+2}{n+2}\right) \frac{1}{k_B^2} + \frac{2(1-s)}{n+2} k_B^n + s + \frac{2}{3}(k - k_B); \tag{IV-23}$$

$$k_B - 2 \leq k \leq k_B \quad \text{(kinematic hardening)}$$

$$k_B - 2\{(1-s) k_B^n + s\} \leq k \leq k_B \quad \text{(isotropic hardening)}$$

(δ) plastic reverse loading (E - $-\infty$)

$$m = \left\{\frac{2}{3} - \frac{2(1-s)}{n+2}\right\} \frac{1}{k_B^2} - \frac{2(1-s)}{n+2} k_B^n + \frac{4}{3} \left\{\frac{(1-s)(1-n)k_B^n}{n+2} - s\right\}$$

$$\times \left\{\frac{k_B - k}{2(1-s)k_B^n + 2s}\right\}^{\frac{n+2}{n-1}} + s \left\{2 \left[\frac{k_B - k}{2(1-s)k_B^n + 2s}\right]^{\frac{2}{n-1}} - \frac{1}{k_B^2} - 1\right\}$$

; no reverse hardening (approximation) (IV-24)

In Fig. IV-5 the nominal stress-engineering strain relation is given for annealed copper. This relation is approximated by 2-parameter power-law hardening as shown in dashed line in the Figure. The values used in equation (IV-20) are; σ_y = 60 MPa, s = 0.85, n = 0.57 and E = 124 GPa. The

corresponding bending moment-curvature relation of equations (IV-21 ~ 24) is plotted in Fig. IV-6. As the moment-curvature relations are expressed in non-dimensionalized form, the equilibrium equations can be also expressed in non-dimensionalized form. Before we nondimensionalize the equations, we can also reduce the system of equations to a single equation by employing the global force equilibrium relations. The relations $T = p\cos(\phi - \theta)$ and $N = p\sin(\phi - \theta)$ satisfies the Eqn.'s (IV-1) and (IV-2) readily, where ϕ is the peel angle. And the Eqn.'s (IV-1) and (IV-3) provide the relation

$$\frac{dT}{ds} + K\frac{dM}{ds} = 0. \qquad \text{(IV-25)}$$

If M is a function of s only through K, then the relation can be expressed in the integral form as,

$$T + KM - \int M\, dK = \text{constant}. \qquad \text{(IV-26)}$$

Then substituting $T = p\cos(\phi - \theta)$ and normalizing K and M by K_e and M_o, we can get

$$\frac{\eta}{3}\cos(\phi - \theta) + km - \int m\, dk = \text{const}. \qquad \text{(IV-27)}$$

The new variable η is a non-dimensionalized peel force defined by

$$\eta = \frac{3P}{k_e M_o} = \frac{6EP}{\sigma_y^2 t} \qquad \text{(IV-28)}$$

Whenever M is a function of s but <u>not</u> through K, then Eqn. (IV-25) has to be used directly. For example, if the adherend deforms elastically from an initial configuration of nonzero curvature and moment, then the governing equation becomes

$$\frac{dk(\bar{s})}{d\bar{s}} + \frac{1}{2}\eta \sin(\phi - \theta) = \frac{dk_o(\bar{s})}{d\bar{s}} - \frac{3}{2}\frac{dm_o(\bar{s})}{d\bar{s}} . \qquad \text{(IV-29)}$$

where $k_o(\bar{s})$ and $m_o(\bar{s})$ are the initial curvature and moment, and $\bar{s} = K_e s$. Although the governing equation is formulated for general peel angle ϕ, our interest is focused in the case of 90° peel test $(\phi = \frac{\pi}{2})$ throughout this report.

B. Analytic Results

In this section, the analysis is given for a elastic perfect plastic adherend . If the adherend remains elastic, we can get the curvature distribution as a function of θ from equations (IV-7) and (IV-27) for $\phi = \frac{\pi}{2}$. The necessary boundary condition is

$$k = 0 \quad \text{for} \quad \theta = \frac{\pi}{2} . \qquad \text{(IV-30)}$$

Then, the curvature is given as

$$k = \{\eta\ (1 - \sin\theta)\}^{1/2} \qquad \text{(IV-31)}$$

The condition to have the adherend elastic everywhere is $k_{max} \leq 1$, so that we can get the relation from equation (IV-31)

$$\eta \leq 1/(1 - \sin\theta_B), \qquad \text{(IV-32)}$$

where θ_B is the base angle of the adherend at the root of the crack. Because we have the relation (IV-6)

$$K = \frac{d\theta}{ds} = K_e\ k = K_e\ \{\eta\ (1 - \sin\theta)\}^{1/2} \qquad \text{(IV-33)}$$

Then,

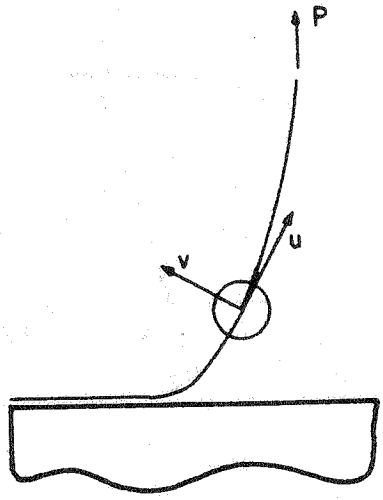

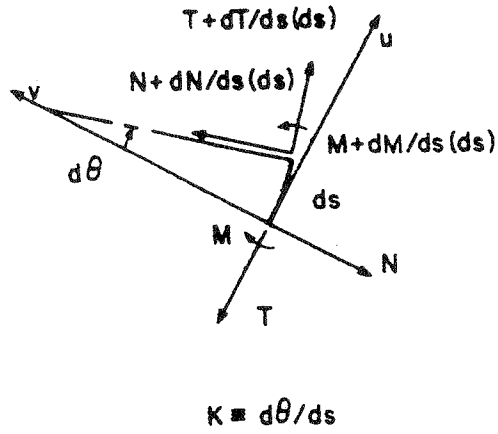

$K \equiv d\theta/ds$

Fig. IV-1

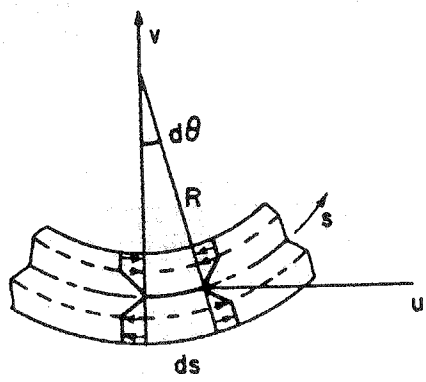

Fig. IV-2

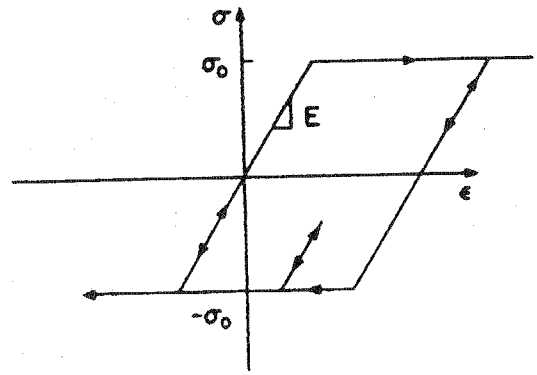

Fig. IV-3

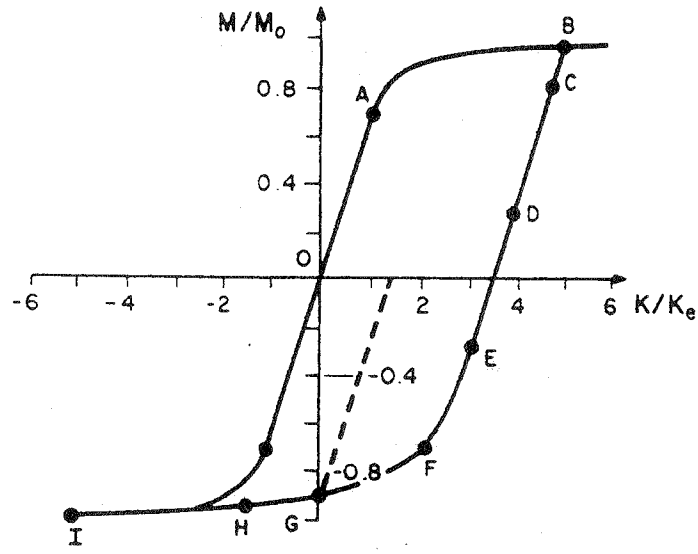

Moment Curvature Relation

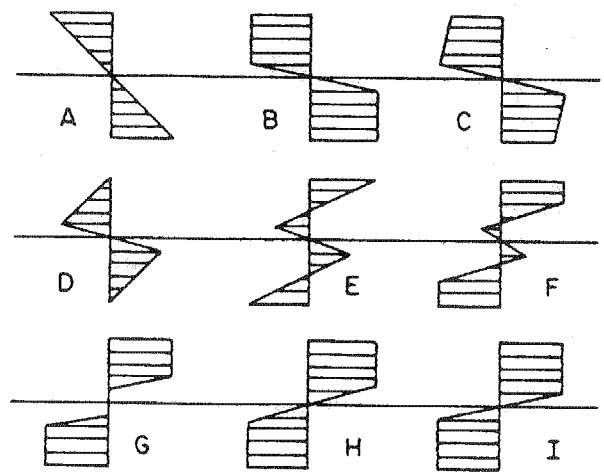

Stress Distribution

Fig. IV-4

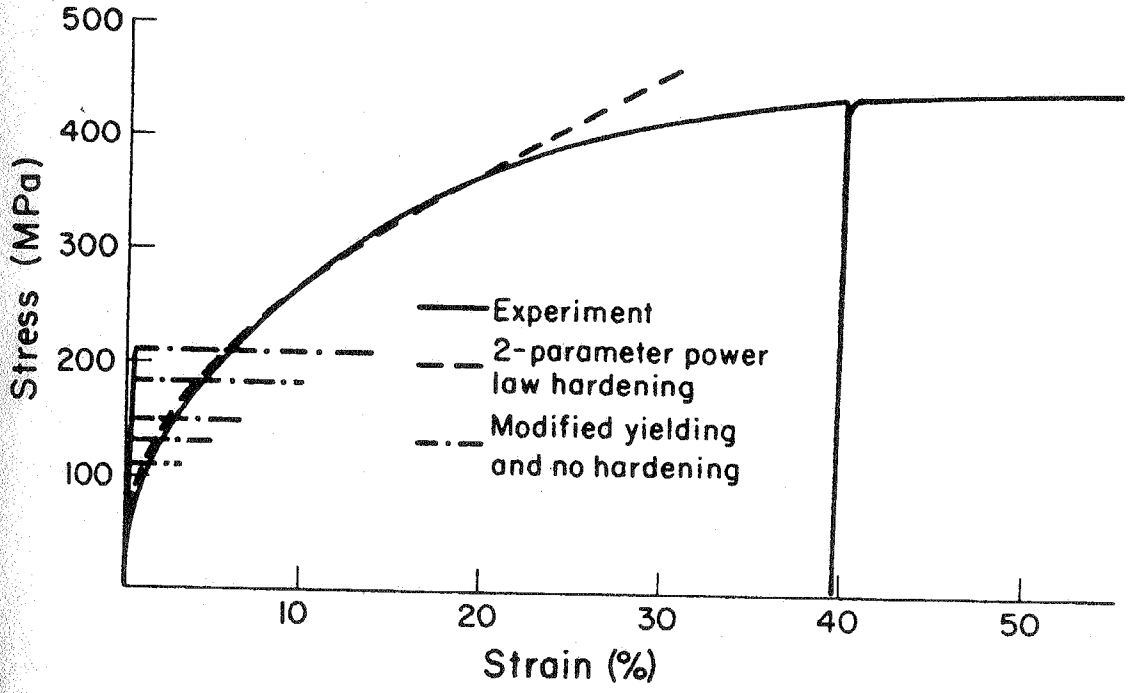
500
400
300
200
100
Stress (MPa)
10
20
30
40
50
Strain (%)
Experiment
2-parameter power law hardening
Modified yielding and no hardening

Fig. IV-5

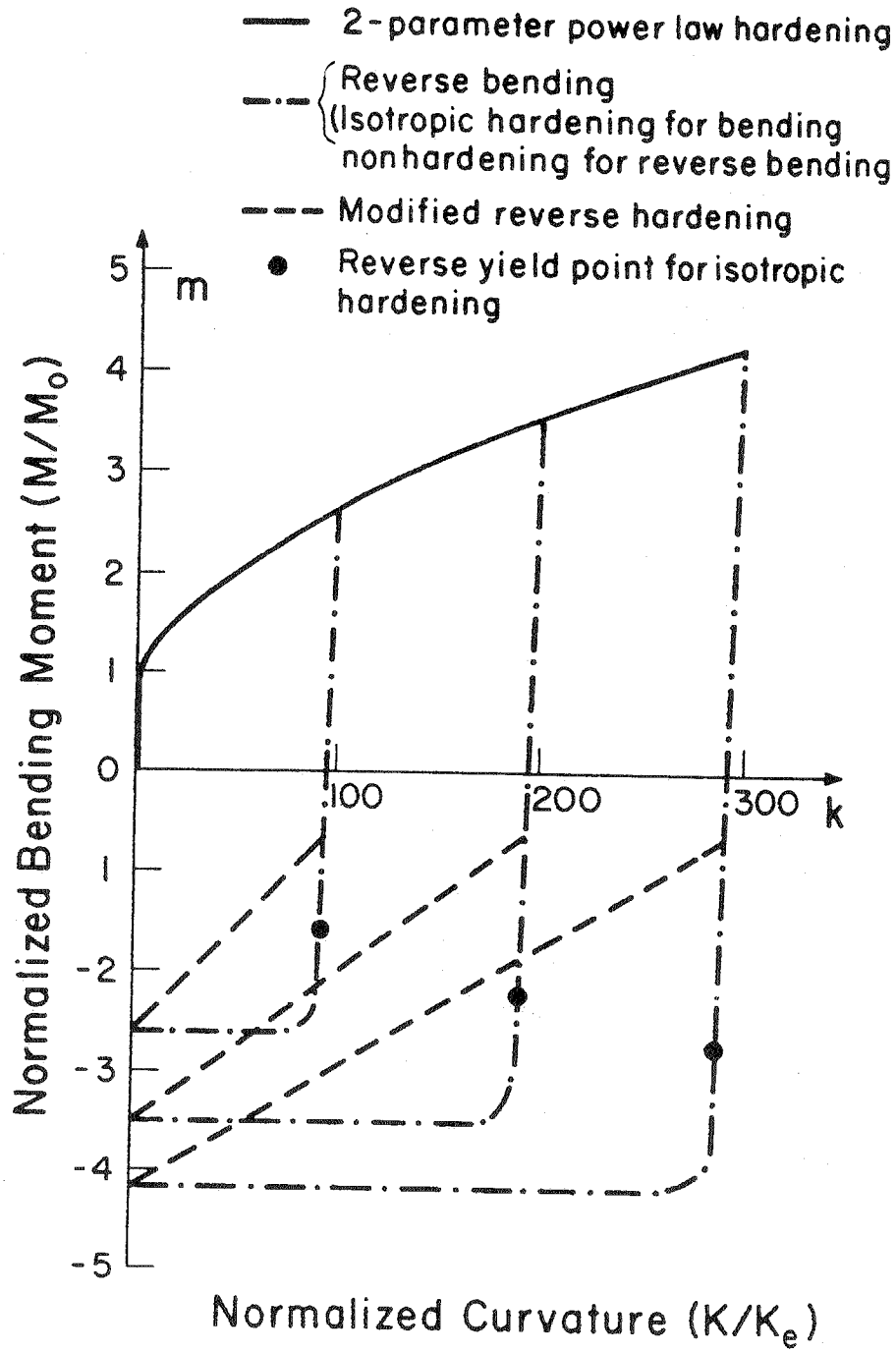
2-parameter power law hardening
Reverse bending
(Isotropic hardening for bending
nonhardening for reverse bending)
Modified reverse hardening
Reverse yield point for isotropic hardening
m
5
4
3
2
1
0
-1
-2
-3
-4
-5
100
200
300
k
Normalized Bending Moment (M/M$_o$)
Normalized Curvature (K/K$_e$)

Fig. IV-6

$$ds = Ke^{-1} \{\eta\ (1 - \sin\theta)\}^{-1/2}\, d\theta, \qquad \text{(IV-34)}$$

$$dx = Ke^{-1} \{\eta\ (1 - \sin\theta)\}^{-1/2} \cos\theta\ d\theta, \qquad \text{(IV-35)}$$

$$dy = Ke^{-1} \{\eta\ (1 - \sin\theta)\}^{-1/2} \sin\theta\ d\theta. \qquad \text{(IV-36)}$$

When $3 > \eta\ (1 - \sin\theta_B) > 1$, plastic bending spreads out from the root of the adherend. The curvature distribution can be obtained from equations (IV-8) and (IV-27), including the patching condition at the elastic-plastic boundary as $k = 1$ and θ be continuous. The curvature distribution is given as,

$$k = 2/\{\eta\ (\sin\theta - 1) + 3\}. \qquad \text{(IV-37)}$$

Then following the similar procedure as for elastic case,

$$ds = \{\eta\ (\sin\theta - 1) + 3\}\ d\theta/(2\ Ke), \qquad \text{(IV-38)}$$

$$dx = \{\eta\ (\sin\theta - 1) + 3\} \cos\theta\ d\theta/(2\ Ke), \qquad \text{(IV-39)}$$

$$dy = \{\eta\ (\sin\theta - 1) + 3\} \sin\theta\ d\theta/(2\ Ke). \qquad \text{(IV-40)}$$

The analysis of elastic case was also given by Drucker [16] for a finite length cantilever beam. Integrating equations (IV-35, 36 and 39, 40), we can get the peel profile as

Elastic Peel Profile; for $0 < \eta \leq 1$

$$X = K_e\ x = \frac{2}{\sqrt{\eta}} \{1 - (1 - \sin\theta)^{1/2}\} \qquad \text{(IV-41)}$$

$$Y = K_e\ y = \frac{2}{\sqrt{\eta}} \left\{1 - (1 + \sin\theta)^{1/2} + \frac{1}{\sqrt{2}} \ln \frac{(\sqrt{2} - 1)(\sqrt{2} + \sqrt{1 + \sin\theta})}{\sqrt{1 - \sin\theta}}\right\}. \qquad \text{(IV-42)}$$

Elastic plastic peel profile; for $1 < \eta < 3$:

<Plastically deformed part>, for $\sin\theta \leq 1 - \frac{1}{\eta}$;

$$X = K_e\, x = \frac{\eta}{4}\left(\sin\theta - 2 + \frac{6}{\eta}\right)\sin\theta \qquad \text{(IV-43)}$$

$$Y = K_e\, y = \frac{\eta}{4}\left\{\theta - \sin\theta\cos\theta - \left(2 - \frac{6}{\eta}\right)(1 - \cos\theta)\right\} \qquad \text{(IV-44)}$$

<Elastically remained part>, for $\sin\theta > 1 - \frac{1}{\eta}$;

$$X = \frac{\eta}{4}\left(\frac{5}{\eta} - 1\right)\left(1 - \frac{1}{\eta}\right) + \frac{2}{\sqrt{\eta}}\left\{\frac{1}{\sqrt{\eta}} - (1 - \sin\theta)^{1/2}\right\} \qquad \text{(IV-45)}$$

$$Y = \frac{\eta}{4}\left[\sin^{-1}\left(1 - \frac{1}{\eta}\right) - \left(1 - \frac{1}{\eta}\right)\frac{1}{\eta}(2\eta - 1)^{1/2} - \left(2 - \frac{6}{\eta}\right)\left\{1 - \frac{1}{\eta}(2\eta - 1)^{1/2}\right\}\right] +$$

$$\frac{2}{\sqrt{\eta}}\left[\left(2 - \frac{1}{\eta}\right)^{1/2} - \frac{1}{\sqrt{2}}\ln\left\{\sqrt{\eta}\,(\sqrt{2} - 1)\left(\sqrt{2} + \sqrt{2 - \frac{1}{\eta}}\right)\right\}\right.$$

$$\left. - (1 + \sin\theta)^{1/2} + \frac{1}{\sqrt{2}}\ln\frac{(\sqrt{2} - 1)\left(\sqrt{2} + \sqrt{1 + \sin\theta}\right)}{\sqrt{1 - \sin\theta}}\right] . \qquad \text{(IV-46)}$$

The peel strip profile, for a non-propagating infinite strip, under increasing loading condition is shown in Fig. IV-7. The displacements are normalized by the elastic limit curvature, K_e. The figure shows a family of profiles for the strip as the load increases, i.e. η increases. The loading parameter, η, is chosen such that the entire strip behaves elastically for $\eta \leq 1$. As the loading parameter increases above 1.0, a portion of the strip plastically deforms. The plastic zone extends from where the strip is attached to the substrate out to a position called the elastic-plastic boundary. Beyond this boundary, the strip deformation remains elastic. The length of the strip which is plastically deformed continues to increase as the load increases. However, when η becomes equal to 3, the bending moment applied to the strip at the point of contact to the substrate becomes the plastic limit bending moment, forming a plastic hinge. For loads of $\eta > 3$ it is anticipated that

the strip will unload elastically leaving the only active plastic deformation confined to the plastic hinge.

Expressing θ as a function of s in equation (IV-46) we can get the relation between the vertical displacement of position $X = K_e S$ and force applied. The relation is shown in Fig. IV-8. The end displacement is normalized by the total physical length of the strip. The solid lines represent the behavior if the material were to remain totally elastic. The dashed lines show the response when the plastic deformation is included. Therefore, the effect of the plastic deformation on the global response can be seen immediately.

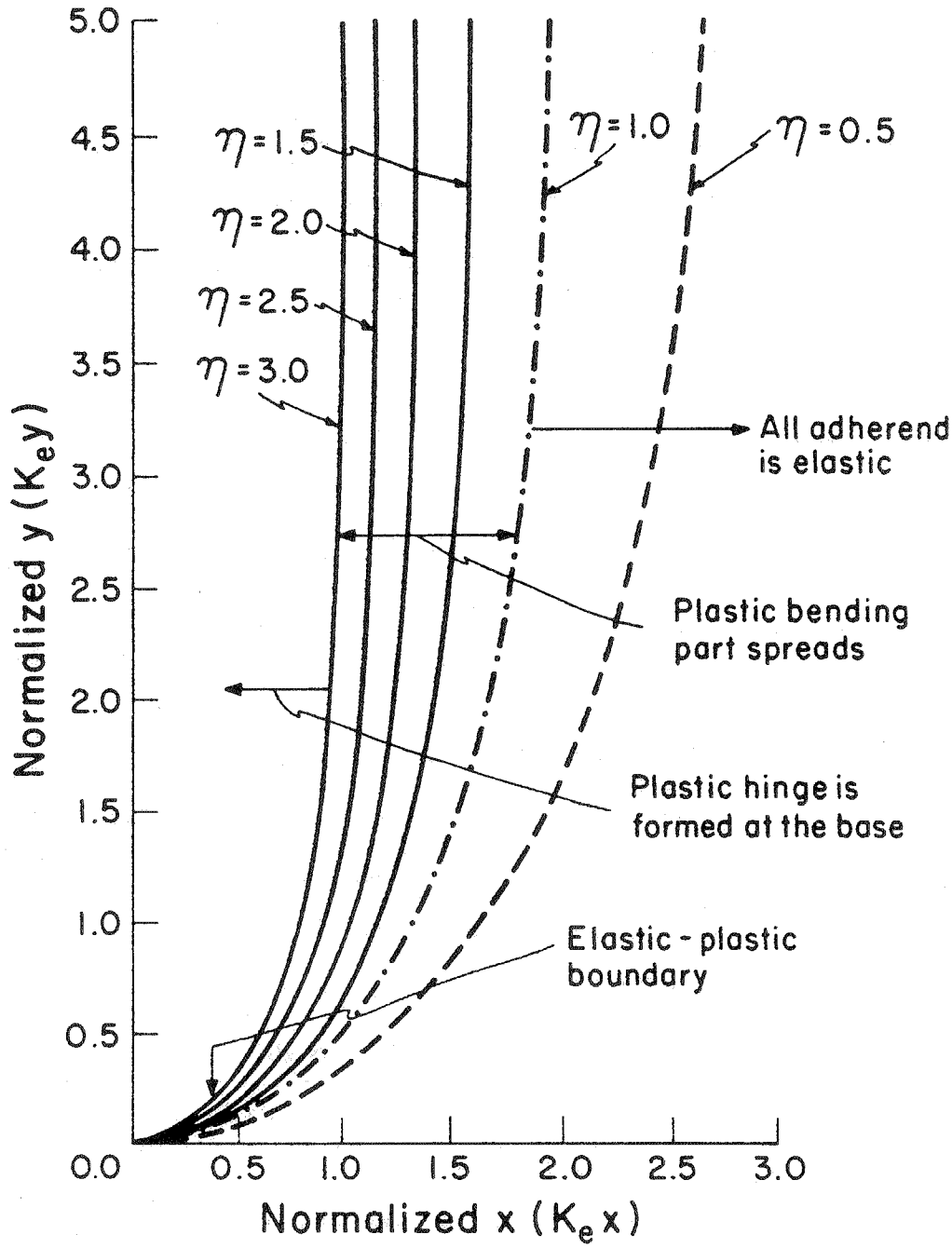
5.0
4.5
4.0
3.5
3.0
2.5
2.0
1.5
1.0
0.5
0.0
0.5
1.0
1.5
2.0
2.5
3.0
Normalized y (K_ey)
Normalized x (K_ex)
η = 1.5
η = 2.0
η = 2.5
η = 3.0
η = 1.0
η = 0.5
All adherend is elastic
Plastic bending part spreads
Plastic hinge is formed at the base
Elastic - plastic boundary

Fig. IV-7

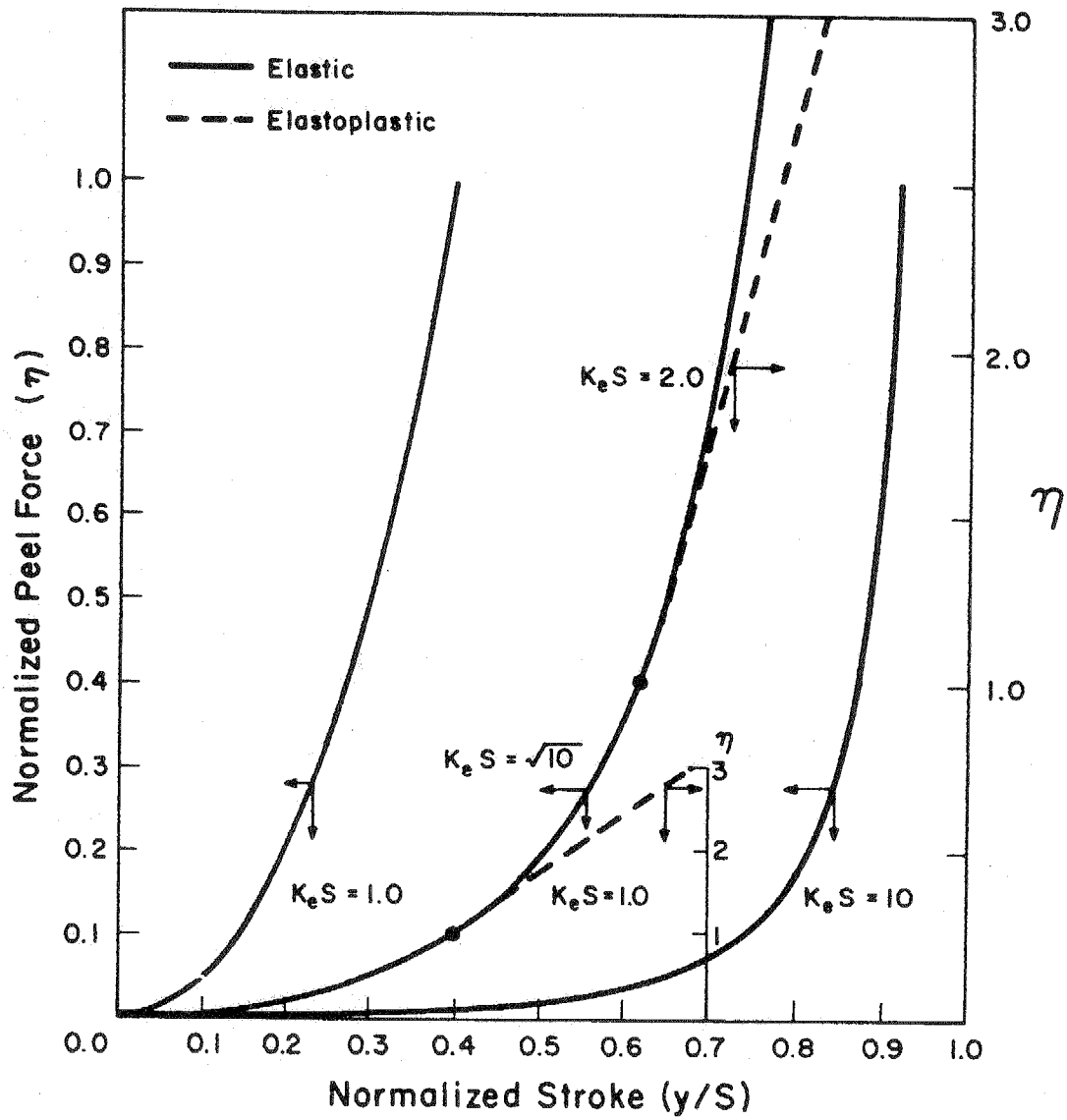
Elastic
Elastoplastic
Normalized Peel Force (η)
Normalized Stroke (y/S)
η
$K_eS = 2.0$
$K_eS = \sqrt{10}$
$K_eS = 1.0$
$K_eS = 1.0$
$K_eS = 10$
0.0
0.1
0.2
0.3
0.4
0.5
0.6
0.7
0.8
0.9
1.0
1
2
3

Fig. IV-8

V. Finite Element Analysis

A. Finite Element Procedure

As mentioned in the Introduction, large displacement finite element analysis has been used to investigate the peel test. The ABAQUS general purpose finite element program developed by Hibbitt, Karlsson and Sorensen Inc., Providence, R.I., was used for the computations.

The geometry analyzed is shown schematically in Fig. V-1. The crack tip was at point 0 (see Fig. V-1) and, in the actual geometry, the part OD of the substrate was aligned to the adherend. The substrate was held fixed along ABCD and the vertical displacement of point E of the adherend was prescribed.

The equilibrium equations were enforced through the virtual work statement

$$\int_V \sigma_{ij}\, \delta D_{ij}\, dV = \int_S t_i\, \delta v_i\, dS + \int_V b_i\, \delta v_i\, dV \qquad \text{(V-1)}$$

where V is the volume of the body and S its surface, $\underset{\sim}{\sigma}$ is the Cauchy stress, $\underset{\sim}{t}$ is the traction vector, $\underset{\sim}{b}$ is the body force per unit volume, $\delta\underset{\sim}{v}$ is an arbitrary virtual velocity variation which vanishes where displacements are prescribed and $\underset{\sim}{D}$ is the deformation rate tensor defined as

$$D_{ij} = \frac{1}{2}\left(\frac{\partial v_i}{\partial x_j} + \frac{\partial v_j}{\partial x_i}\right), \qquad \text{(V-2)}$$

$\underset{\sim}{x}$ being the current position of a material point. In equations (V-1) and (V-2) and for the rest of the paper all tensor components are given with respect to a fixed rectangular coordinate system.

Both the adhesive and the adherend were modeled as elastic-plastic materials. The constitutive law used represents the J_2 flow theory and accounts for rotation of the principal axes; its form is

$$\overset{\nabla}{\tau}_{ij} = \frac{E}{1+\nu}\left(\delta_{ik}\,\delta_{j\ell} + \frac{\nu}{1-2\nu}\,\delta_{ij}\,\delta_{k\ell} - \frac{1}{\frac{2h}{3}\frac{1+\nu}{E} + 1}\,\frac{3\,\sigma'_{ij}\,\sigma'_{k\ell}}{2\bar{\sigma}^2}\right) D_{k\ell} \qquad \text{(V-3)}$$

for plastic loading, and

$$\overset{\nabla}{\tau}_{ij} = \frac{E}{1+\nu}\left(\delta_{ik}\,\delta_{jk} + \frac{\nu}{1-2\nu}\,\delta_{ij}\,\delta_{k\ell}\right) D_{k\ell} \qquad \text{(V-4)}$$

for elastic loading or any unloading, where E is Young's modulus, ν is Poisson's ratio, $\underset{\sim}{\tau}$ is the Kirchoff stress defined by

$$\underset{\sim}{\tau} = J\,\underset{\sim}{\sigma}\,, \qquad \text{(V-5)}$$

where J is the ratio of volume in the current state to volume in the stress-free state, δ_{ij} is the Kronecker delta,

$$\tau'_{ij} = \tau_{ij} - \frac{1}{3}\,\delta_{ij}\,\tau_{kk}, \qquad \bar{\tau}^2 = \frac{3}{2}\,\tau'_{ij}\,\tau'_{ij}, \qquad \text{(V-6)}$$

h is the slope of the uniaxial Kirchoff stress versus logarithmic plastic strain curve, and the superposed ∇ denotes the Jaumann or co-rotational stress-rate. In equations (V-3) and (V-4), $\overset{\nabla}{\underset{\sim}{\tau}}$ is chosen rather than $\overset{\nabla}{\underset{\sim}{\sigma}}$ because the finite element formulation leads then to a symmetric stiffness matrix. The difference between the two formulations is, in any case, of order stress divided by elastic modulus compared to unity [17].

Introducing the finite element interpolation, the equilibrium equations obtained by discretizing the virtual work equation can be written symbolically as

$$F^N\,(u^M) = 0 \qquad \text{(V-7)}$$

where F^N is the nodal force component conjugate to the Nth nodal variable in the problem and u^M is the value of the Mth nodal variable. The basic problem is to solve the nonlinear equations (V-7) throughout the history of interest.

Since our problem was history dependent the solution was developed by a series of increments and Newton's method was used to solve the equilibrium equations at any time. The constitutive equations were integrated in time by the backward Euler method which is unconditionally stable and produces a symmetric material stiffness matrix for the Newton solution of the overall equilibrium equations. More details on the solution procedure can be found in reference [18].

The finite element mesh in the near crack tip region is shown in Fig. V-2 in its undeformed configuration. A total of 906 nodes and 149 plane strain 8-noded elements with 4 integrations of the stiffness were used [19]. The elements used had an independent interpolation for the dilatation rate in order to avoid artificial constraints on incompressible modes [20].

In our calculations we modeled a peel test in which the adherend was made of copper and polyimide was used as substrate. The constitutive behavior of copper was described by E = 124 GPa, ν = 0.3 and the $\tau - \bar{\varepsilon}^p$ curve shown in Fig. IV-5; in addition, isotropic hardening was used to describe the constitutive behavior of the material. Polyimide was modeled by an elastic perfectly-plastic material with E = 4 GPa, ν = 0.3 and a tensile yield stress Y = 65 MPa.

In our calculations the thickness of the adherend was t = 50 μm, 100 μm, and 200 μm; in addition the dimensions of the geometry analyzed were a = 100 mm, b = 15 mm, c = 20 mm, and d = 20 mm.

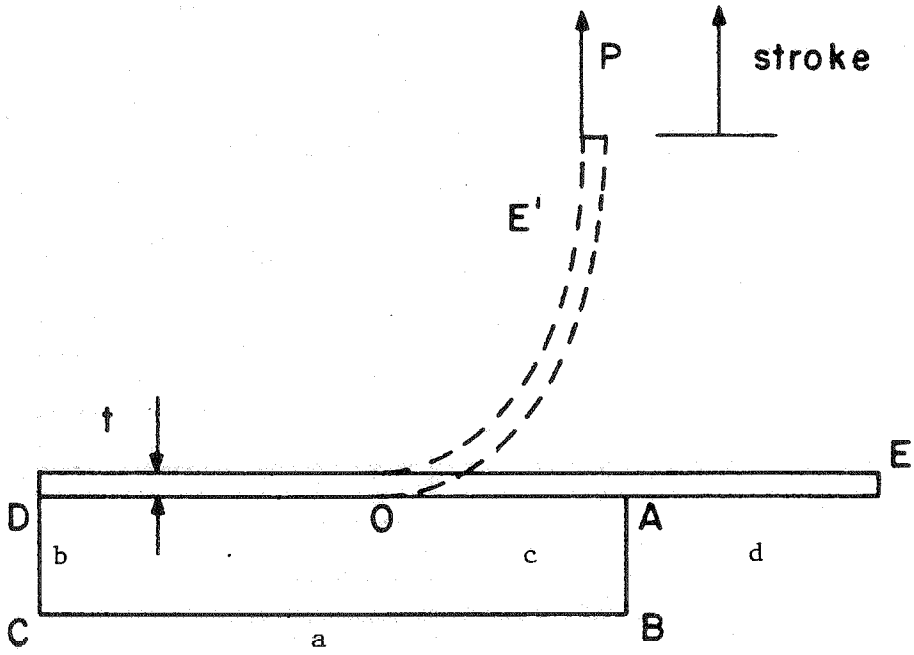

Fig. V-1

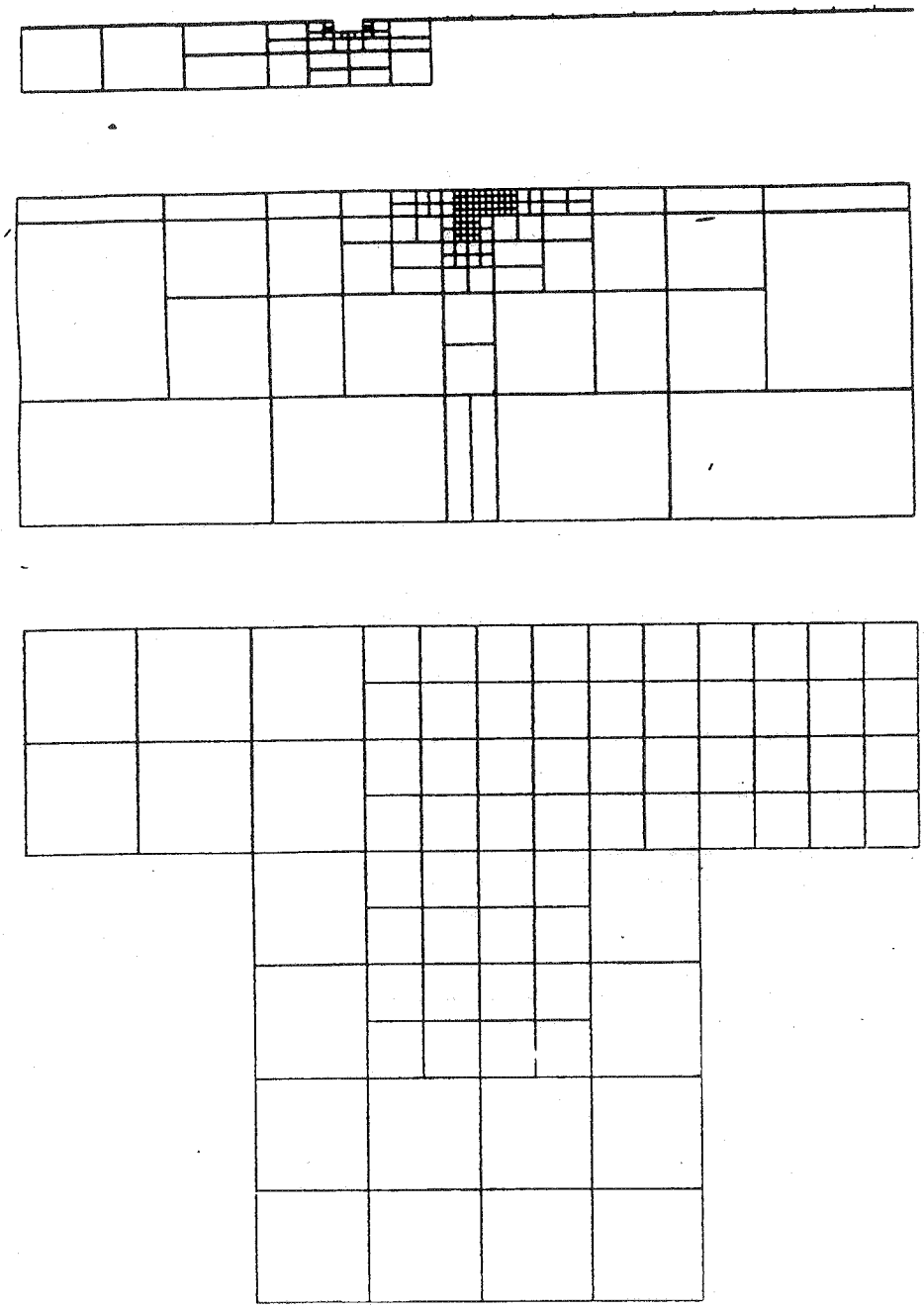

Fig. V-2(a)

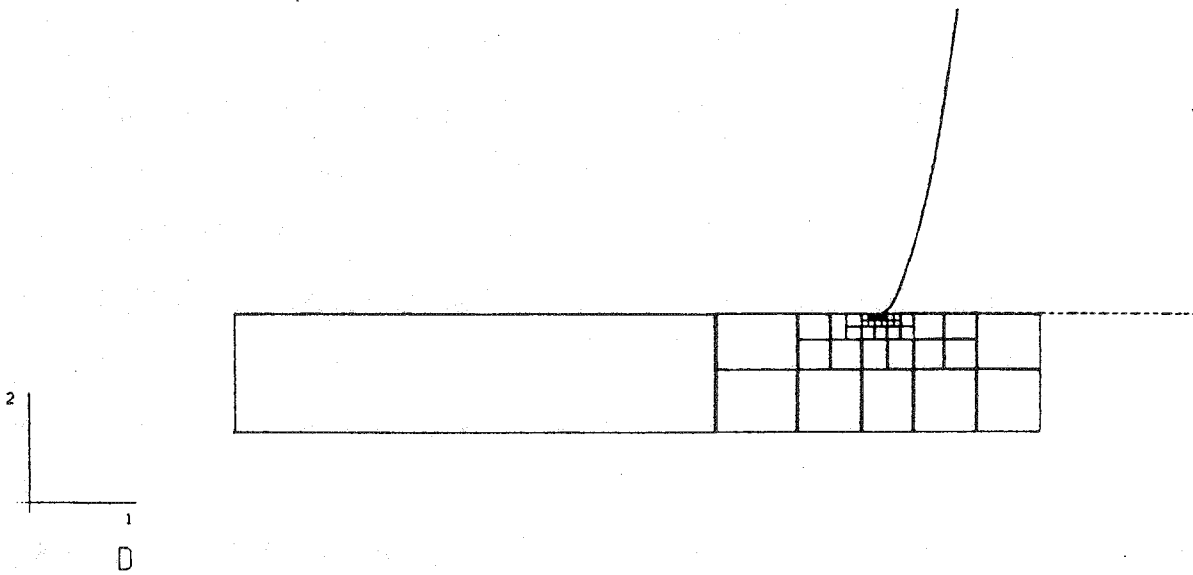
2
1
D
STEP 12 INCREMENT 9
ABAQUS VERSION 4-5-138

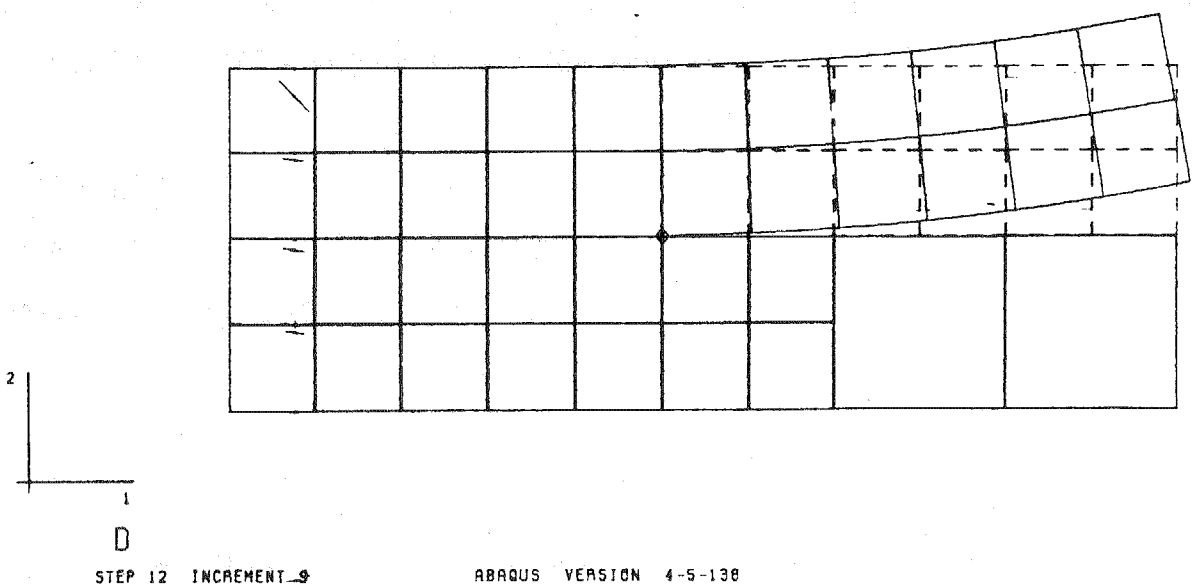
2
1
D
STEP 12 INCREMENT 9
ABAQUS VERSION 4-5-138

Fig. V-2(b)

B. Numerical Results

In Fig. V-3, the configuration of deformed meshes near the interfacial crack tip is shown for purely elastic deformation. The adherend has Young's modulus of 12.4 GPa and the substrate has the modulus of 4 GPa. In this case, there is a stress singularity at the crack tip. However, even for extreme cases of stress intensity, the deformation of the adherend shows basically a simple bending pattern. These results partly support the use of simple bending assumption in one dimensional approximation of the goverening equation of adherend deformation. In Fig. V-4, the successive configuration of near-tip deformation for elastic perfect plastic adherend on an elastic substrate. The configuration was calculated, controlling the end displacement of the adherend. For these two extreme cases of Fig. V-3 and 4, the Young's modulus was artificially reduced to 1/10 of the modulus of copper in order to enhance the deformation. In Fig. V-4, fully plastic deformation is already spread across the thickness of the adherend in the third configuration. After the plastic hinge is formed, the deformation pattern has a noticeable shear mode on top of simple bending mode at very near the root of the crack.

In Fig. V-5 ~ 11, the constitutive relation of the copper adherend was modeled elastic and linear hardening material. Throughout the analysis in this section, the yield surface is assumed to follow isotropic hardening rules. For this linear hardening model, the yield stress was assumed 60 MPa and the Young's modulus was 124 GPa. The linear hardening was assumed in nominal stress and logarithmic strain axis for uniaxial stress test. The slope of the linear hardening coefficient was determined by connecting yield point and the point (0.55, 480 MPa) in the stress-strain plane. The profile of the adherend is shown for 3 stages of loading (1), (2) and (3). The correspnding elastic plastsic boundaries and the load levels are indicated in

Fig. V-6. The whole plastic deformation part is shown for the stage (3) in Fig. V-7. In Fig. V-8 and 9, the equivalent plastic strain and stress contour is shown near the root of the crack. As shown in these figures, the deformation mode is basically simple bending mode. In addition, the penetration length of plastic deformation region into the bonded adherend is only order of the thickness of the adherend. Therefore the process of bending is highly localized near the root of the crack. The interfacial normal stress distribution is shown in Fig. V-10. The result shows that the interfacial normal stress changes from tension to compression at distance of approximately half of the thickness from the root of the crack. As shown in this figure, the force couple is generated basically within the distance of thickness. The normal stress distribution becomes negligible beyond the distance of 6 times of the thickness. In Fig. V-11, the peel force-peel stroke relation is predicted up to onset of peel propagation. As shown in this figure, there is a distinct kink at peel stroke of approximately 7.4 mm. Up to this kink the peel force - peel stroke relation is almost linear. It is believed that, at this point, the adherend becomes fully plastic across the thick near the crack tip. Beyond the peel stroke of 35 mm, the geometric nonlinear deformation caused by large deflection makes the curve much steeper. This portion of the curve is predominantly observed in strong adhesion peel test.

In Fig's. V 12~14, numerical result is given for real stress-strain relation as shown in Fig. IV-5. The yield surface behavior was again assumed to follow isotropic hardening rule. The thickness of the adherend is taken 50 μm. The free adherend length is again set to be 40 mm. In Fig. V-12 the peel profile is shown for peel stroke Δ = 15, 30, 35.58 and 39.70 mm. As shown in this figure, the adherend shows more curvature than the configuration shown in Fig. V-5, because the adherend is thinner. Furthermore the profile

of stroke 39.70 mm shows the curvature inversion at about 3.8 mm away from the root. This curvature inversion caused by large deflection preset the moment-curvature distribution, along the adherend, similar to the distribution of steadily propagating peel profile. The steady state peeling is discussed in Chapter VI. This curvature inversion is believed to provide smooth transition of peel force-stroke relation from the initiation of peel propagation to the steady state. In Fig. V-13, the normal stress distribution at the interface is shown. The stress changes from tension to compression at the distance of approximately half of the thickness from the root of the crack. In Fig. V-14, shear stress distribution is given along the interface. As shown in this figure, the shear stress distribution is similar in magnitude to the normal stress distribution. This result shows that the 90° peel test provides mixed mode failure at the interface. This indicates that the energy method introduced in Chapter III deals with total energy release rate. Recent experimental study on joint failure [21] shows that the total energy release rate controls the interfacial fracture. Therefore the energy approach introduced in this report is more relevant than debonding criteria based on normal stress at the interface.

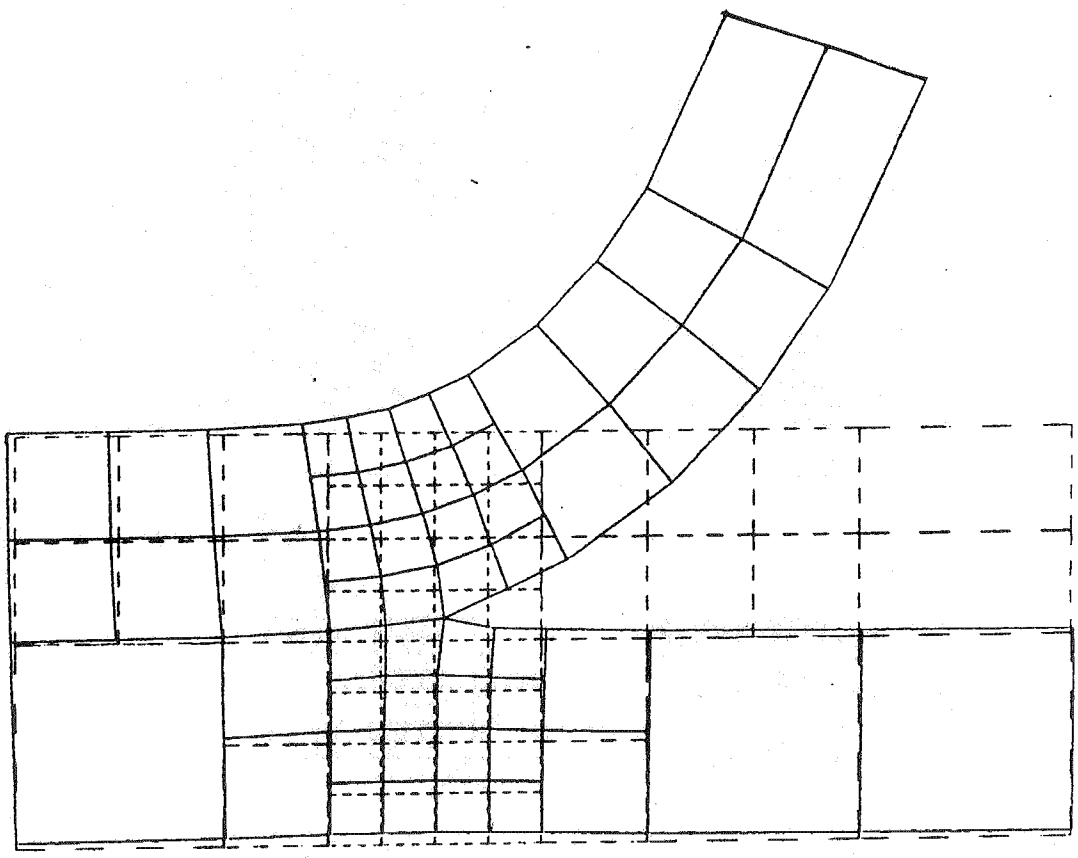

Elastic Peeling

Fig. V-3

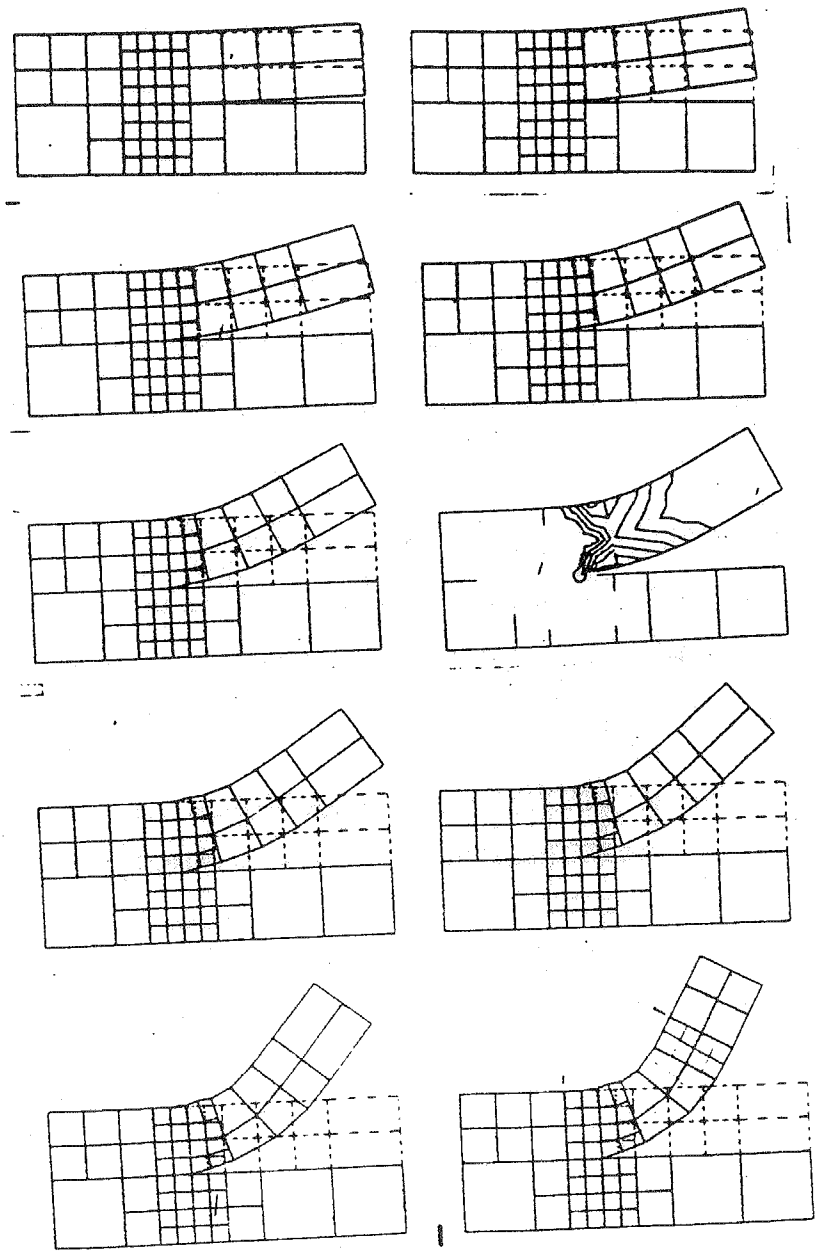

Elastic-Perfect Plastic

Fig. V-4

Elastic-Linear Hardening

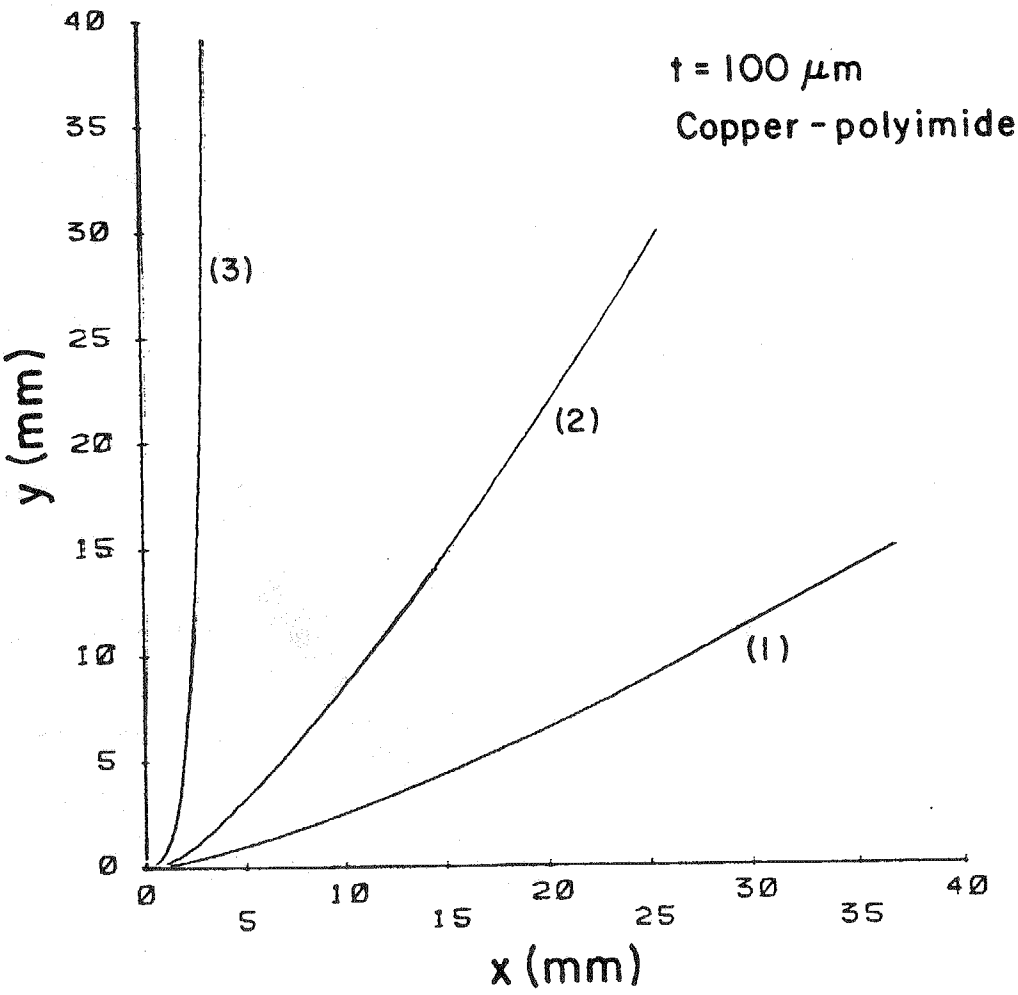

Fig. V-5

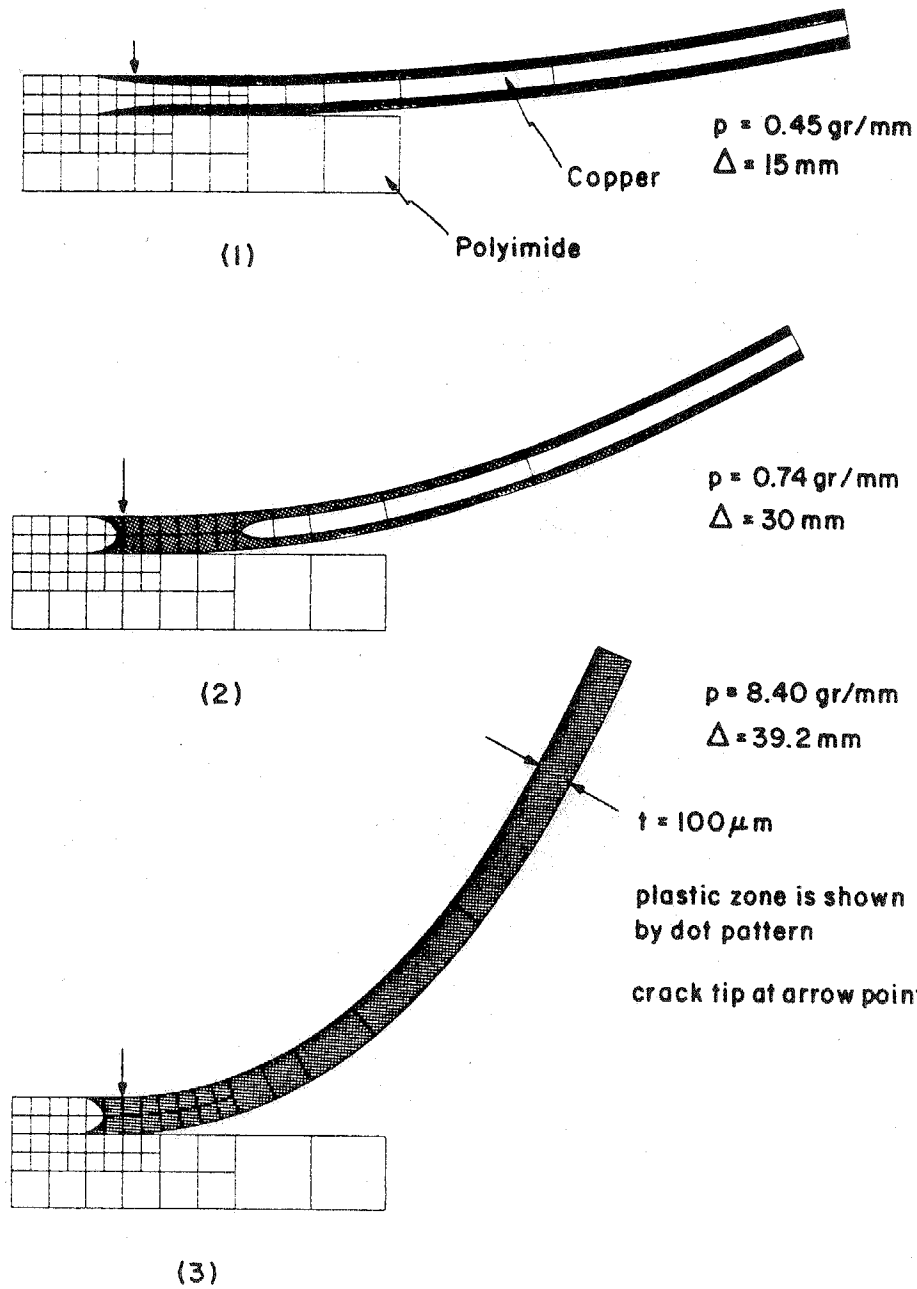
p = 0.45 gr/mm
Δ = 15 mm
Copper
Polyimide
(1)
p = 0.74 gr/mm
Δ = 30 mm
(2)
p = 8.40 gr/mm
Δ = 39.2 mm
t = 100 μm
plastic zone is shown
by dot pattern
crack tip at arrow point
(3)

Fig. V-6

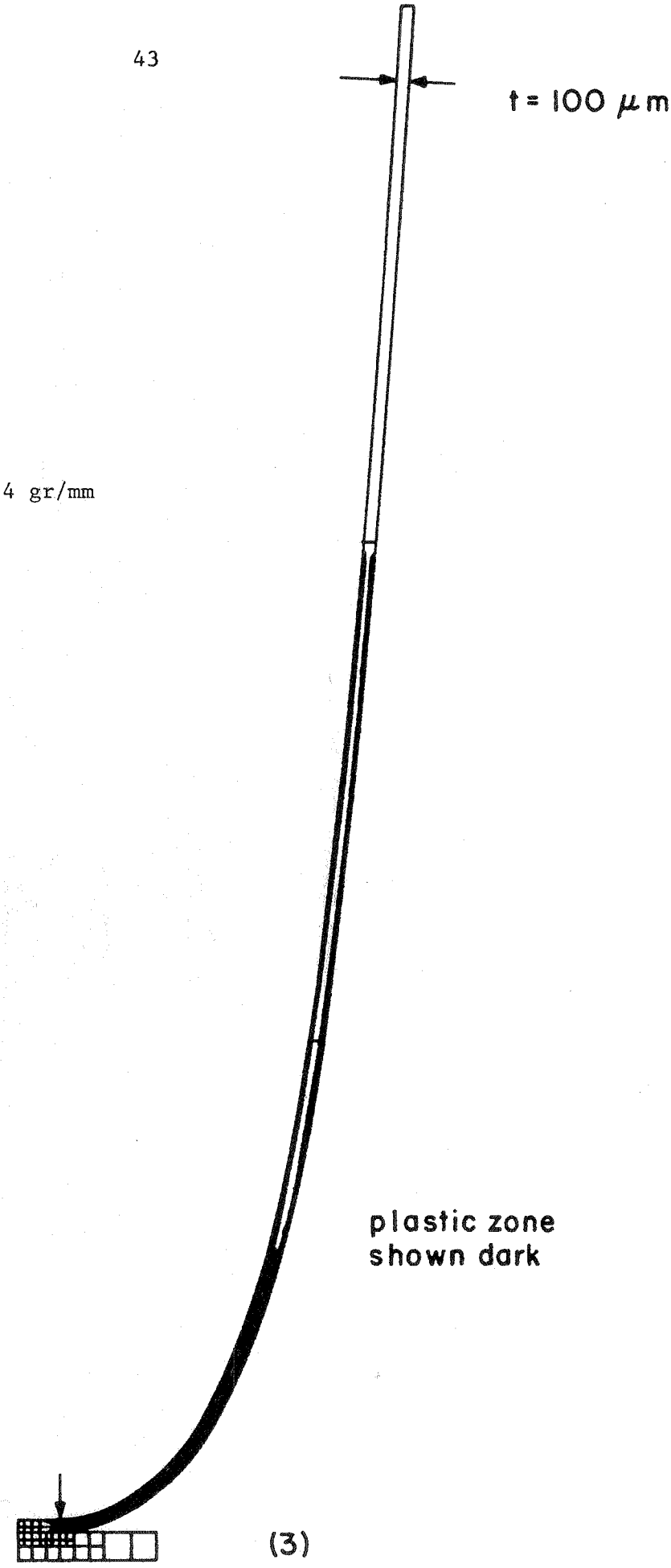

Fig. V-7

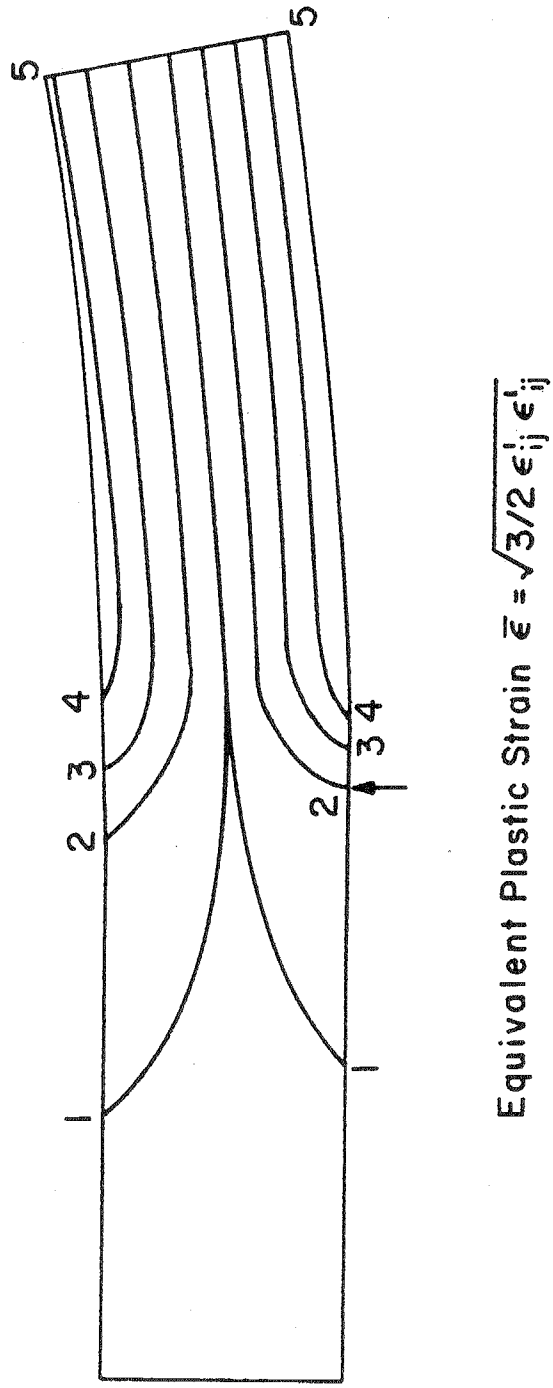
5
5
4
3
2
2
3
4
1
1
Equivalent Plastic Strain $\bar{\epsilon} = \sqrt{3/2\,\epsilon'_{ij}\,\epsilon'_{ij}}$

Fig. V-8

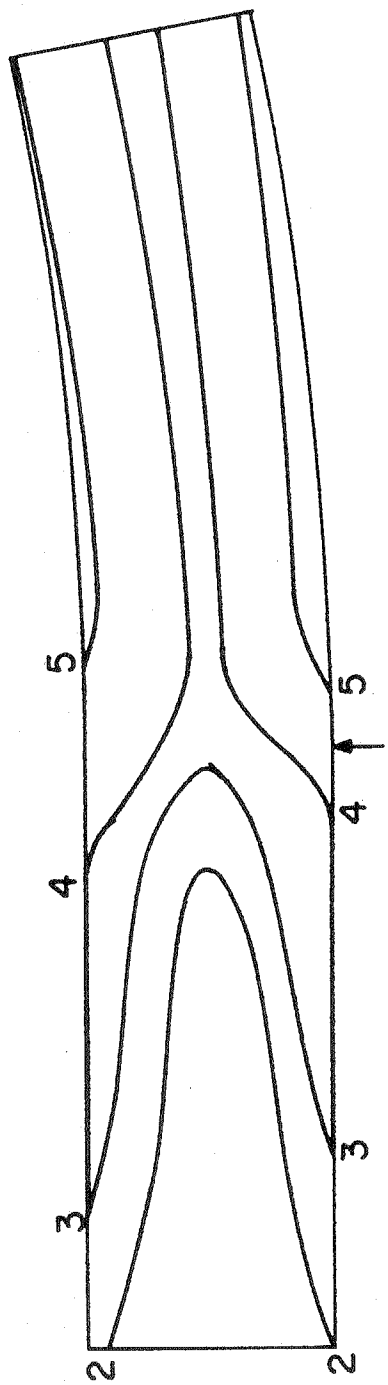

Equivalent Shear Stress $\bar{\sigma} = \sqrt{3/2\, \sigma'_{ij}\, \sigma'_{ij}}$

Fig. V-9

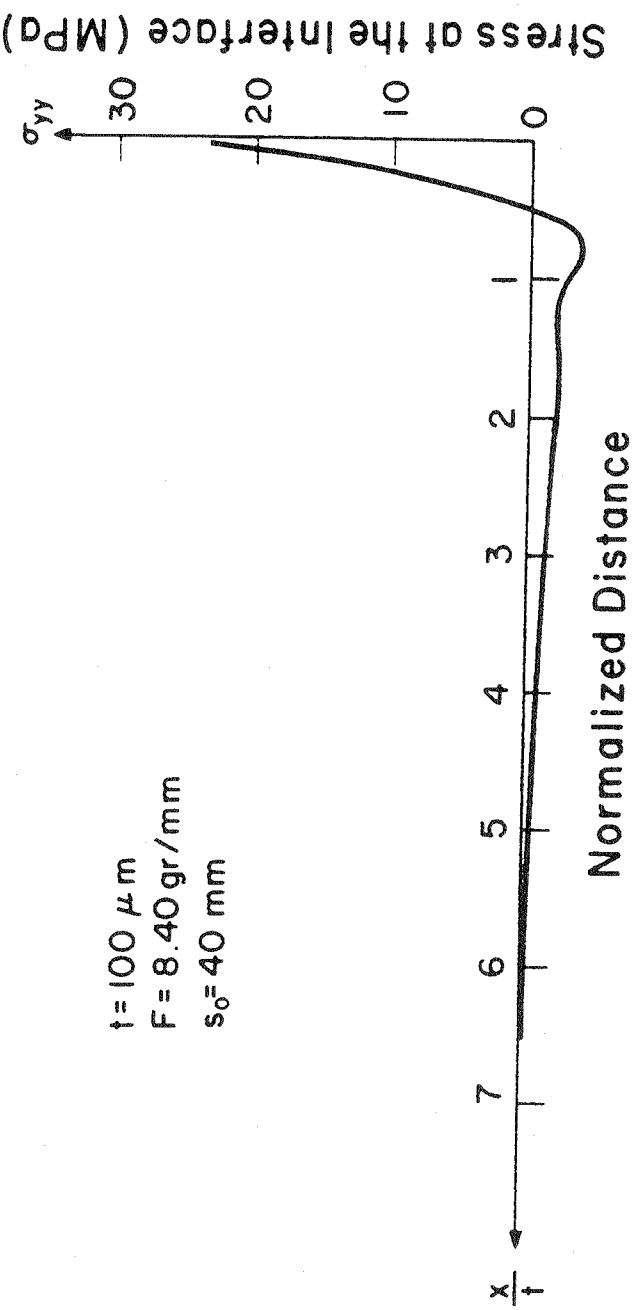
Stress at the Interface (MPa)
σ_{yy}
30
20
10
0
1
2
3
4
5
6
7
Normalized Distance
$\frac{x}{t}$
t= 100 μm
F= 8.40 gr/mm
s_0= 40 mm

Fig. V-10

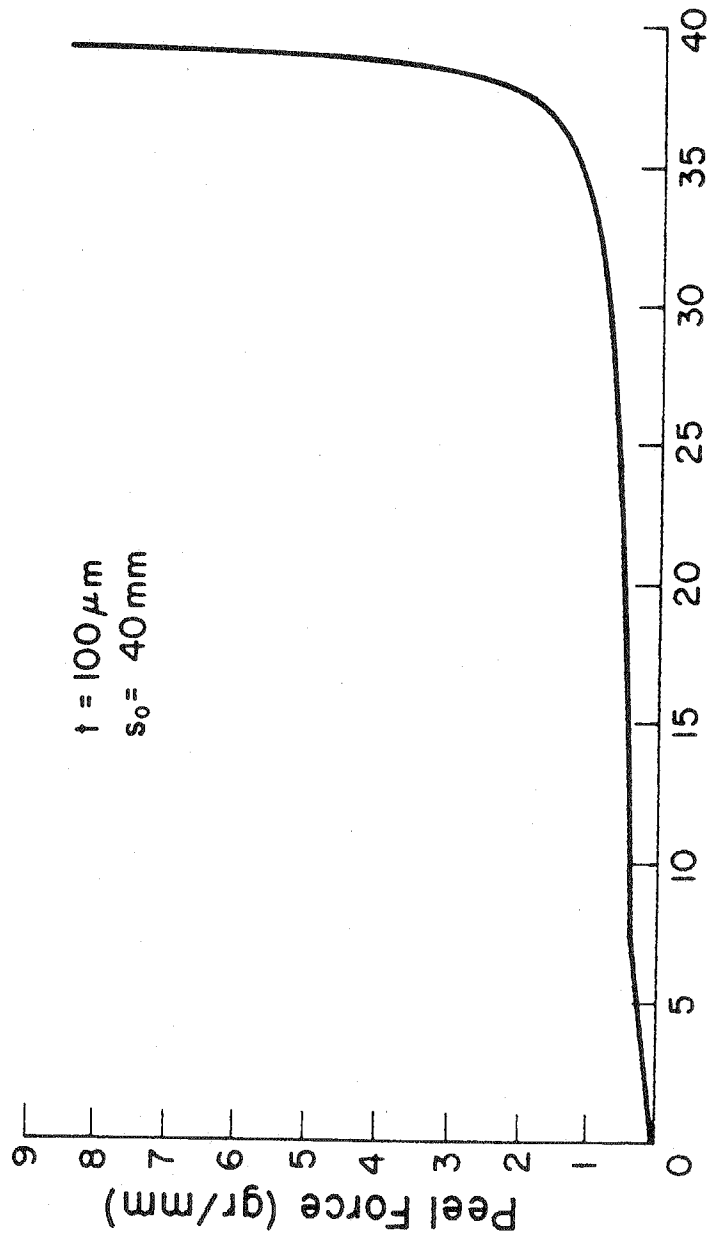
t = 100 μm
s₀ = 40 mm
Peel Force (gr/mm)
0
1
2
3
4
5
6
7
8
9
Peel Stroke (mm)
0
5
10
15
20
25
30
35
40

Fig. V-11

Real Hardening

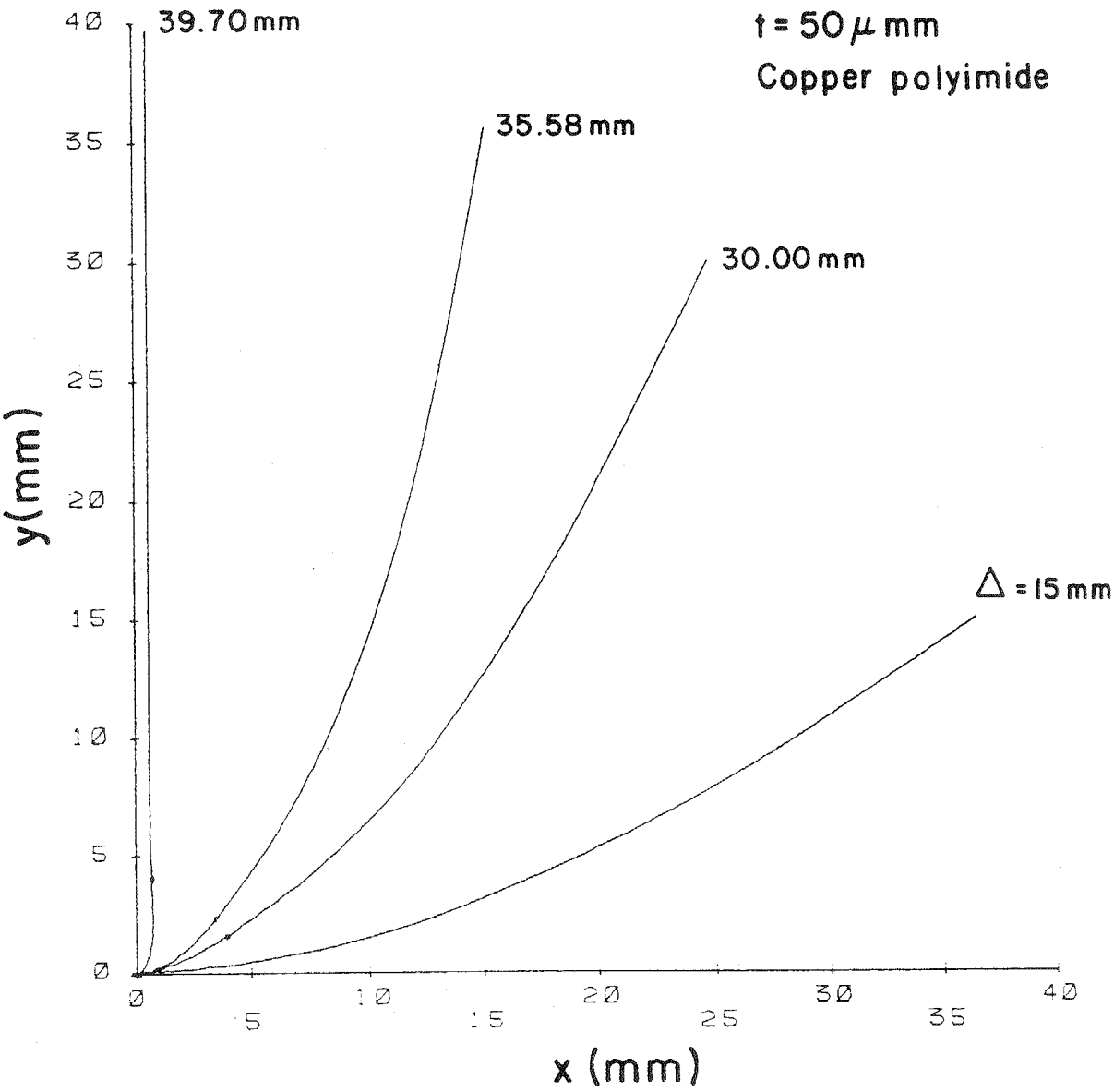

Fig. V-12

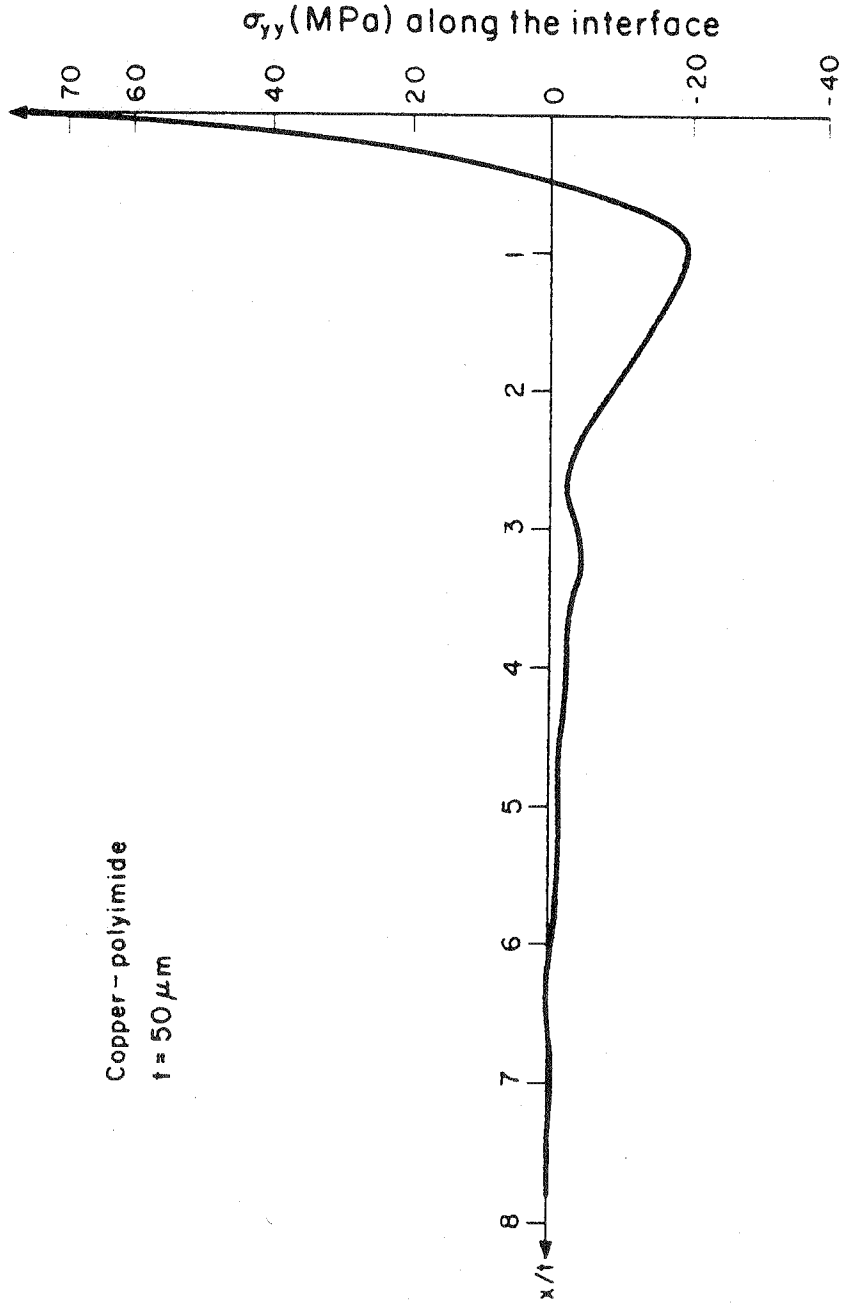
σ_{yy}(MPa) along the interface
70
60
40
20
0
-20
-40
1
2
3
4
5
6
7
8
x/t
Copper-polyimide
t = 50 μm

Fig. V-13

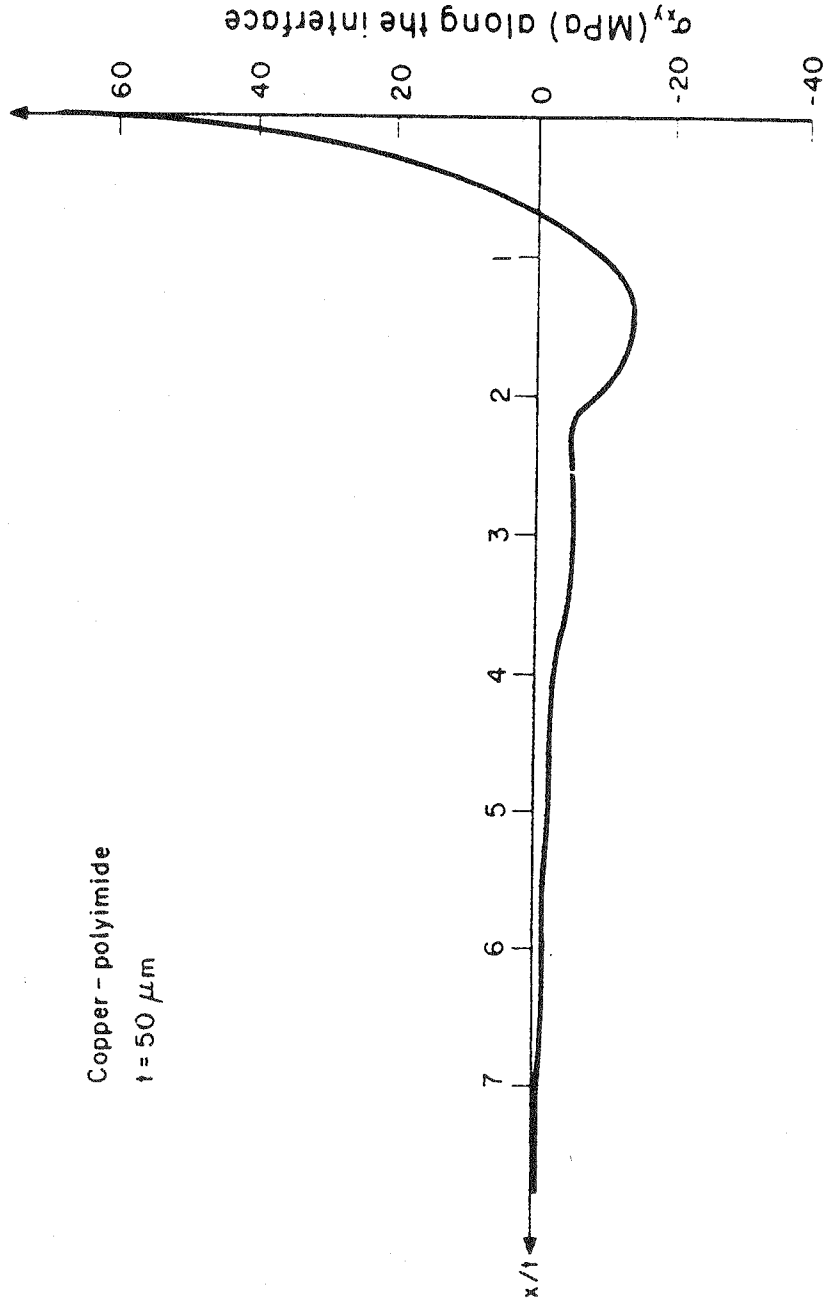
σ_y(MPa) along the interface
60
40
20
0
-20
-40
1
2
3
4
5
6
7
x/t
Copper - polyimide
t = 50 μm

Fig. V-14

VI. Analysis of Steady State Peeling

After the debonding begins to propagate in a 90° peel test, the peel force approaches a steady-state one. The steady-state peel force is referred to be the peel strength of the joint. Therefore the analysis of steady-state peel propagation is important. An approximate analysis of steady-state peel propagation for an elastic-plastic adherend was first made by Chen, et al [22]. However, they assumed that if the plastically deformed adherend is unloaded, the adherend recoils back to a circular arc of a constant curvature. However this assumption does not include the reverse-bending effect in the analysis. In this chapter, the analysis of steady-state peel propagation includes the effects of reverse bending and the analysis is applied to an energy method of describing adhesion-bond strength.

When the peeling is in steady state, the configuration maintains to be in same shape. The configuration of the steady-state peeling is shown in Fig. VI-1(a). As shown in the figure the adherend has various sections of bending and unbending process. The boundaries of the various sections are denoted by O,A,B,C,D,E, and F. The corresponding distribution of moment and curvature is indicated in the moment-curvature diagram of Fig. VI-1(b). As indicated in these figures, the adherend is in elastic-bending stage in the section O-A, plastic-bending stage in A-B, elastic-unloading stage in B-D, plastic-reverse-bending stage in D-E and the elastic-unloading-of-reverse-bending stage in E-F.. If the adherend is set free of peel force, the adherend will recoil to have curvature distribution as shown with the dashed line in Fig. VI-1(a). The section B-D will recoil to have a constant curvature of C. The unloaded section A-B and D-E will have gradually varying curvature distribution. The section E-F will be unloaded to have another constant curvature of F.

Because the configuration maintains same shape, a material point of the adherend will experience the bending moment and curvature along O-A-B-C-D-E-F. Therefore, the internal work expenditure of the adherend per unit advance of peeling is $M_o K_e$ multiplied by the area enclosed by O-A-B-C-D-E-F-O. In real experiments, however, the length of section B-F changes as the peel propagates; the moment-curvature distribution in the adherend will be slightly changed. Therefore, it is more realistic to take the area O-A-B-C-D-E-O than O-A-B-C-D-E-F-O. In this case it is assumed that the bending moment at E is maintained constant to have steady-state configuration. In this energy approach, the critical factor that determines the work expenditure is the maximum curvature k_B. Once k_B is obtained, the work expenditure (Mo Ke x area) can be easily calculated, because the moment-curvature relation is known for the adherend. The k_B can be obtained from the equilibrium equation and the inter-boundary matching conditions. These analysis of peeling is analogous to those of asymptotic behavior of near tip plasticity of a crack moving in quasi-static manner [23].

The close form solution is obtained for elastic-perfect plastic material model in the following. The governing equilibrium equation is given for general elasto-plastic bending, as

$$\frac{\eta}{3} \sin\theta + km - \int m(k)\, dk = \text{constant}. \qquad \text{(VI-1)}$$

Then the curvature distribution of section B-D of elastic perfect adherend is obtained by employing moment-curvature relation of equation (IV-9) and the boundary condition, $\theta = \theta_B$ and $k = k_B$ at B. Then,

$$k = \{k_B^2 + \eta(\sin\theta_B - \sin\theta)\}^{1/2} \qquad \text{(VI-2)}$$

Similarly, applying the moment-curvature relation, equation (IV-10), and the boundary condition $\theta = \frac{\pi}{2}$, $k = 0$ at E, the curvature distribution is obtained for section D-E as, for $k_B \geq 2$,

$$k = \{k_B^3 \, \eta(1-\sin\theta)\}^{1/2} / [2\sqrt{2} + \{k_B \, \eta(1-\sin\theta)\}^{1/2}] \tag{VI-3}$$

Then, if the patching condition at D is employed as $\theta = \theta_D$, $k = k_D = k_B - 2$, for $k_B \geq 2$, the curvature k_B becomes

$$k_B = 1 + \frac{\eta}{12}(1-\sin\theta_B) + [\{1 + \frac{\eta}{12}(1-\sin\theta_B)\}^2 - \frac{4}{3}]^{1/2} \tag{VI-4}$$

and

$$\sin\theta_D = \sin\theta_B + \frac{4}{\eta}(k_B - 1). \tag{VI-5}$$

Then, the maximum curvature and moment for the whole range of k_B, becomes

For $0 \leq k_B < 1$; elastic loading and unloading,

$$k_B = \{\eta(1-\sin\theta_B)\}^{1/2} \tag{VI-6}$$

$$m_B = \frac{2}{3}\{\eta(1-\sin\theta_B)\}^{1/2} \tag{VI-7}$$

For $1 \leq k_B < 2$; elasto plastic loading and elastic unloading,

$$k_B = \{\eta(1-\sin\theta_B)\}^{1/2} \tag{VI-8}$$

$$m_B = \frac{1}{3}\{3 - \frac{1}{\eta(1-\sin\theta_B)}\} \tag{VI-9}$$

For $2 < k_B$; elastoplastic loading and unloading

$$k_B = 1 + \frac{\eta}{12}(1-\sin\theta_B) + [\{1 + \frac{\eta}{12}(1-\sin\theta_B)\}^2 - \frac{4}{3}]^{1/2} \tag{VI-10}$$

$$m_B = \frac{1}{3}(3 - \frac{1}{k_B^2}) \tag{VI-11}$$

These maximum curvature and moment are shown as a function of η in Fig. VI-2. Then the work expenditure, ψ , per unit advance of peeling is by

$$\psi = M_o K_e \int_{\ell p} m(k)\, dk \qquad \text{(VI-12)}$$

where ℓp indicates loading path O-A-B-C-D-E on moment-curvature plane (Fig. VI-1(a)). In addition the residual strain energy production rate, $\frac{d\Phi}{d\ell}$, can be obtained by calculating the complementary plastic work on the moment curvature plane. In the bending of elastic-perfect plastic adherend, the complementary plastic work caused by geometric hardening is identical to the stoned residual strain energy. Therefore ψ and $\frac{d\Phi}{d\ell}$ are given as following.

For $0 \leq k_B \leq 1$,

$$\psi = 0 \qquad \text{(VI-13)}$$

$$\frac{d\Phi}{d\ell} = 0. \qquad \text{(VI-14)}$$

For $1 \leq k_B \leq 2$,

$$\psi = M_o K_e \left(\frac{2}{3k_B} + \frac{k_B^2}{3} - 1\right) \qquad \text{(VI-15)}$$

$$\frac{d\Phi}{d\ell} = M_o K_e \left(\frac{k_B^2}{3} - k_B - \frac{1}{3k_B} + 1\right) \qquad \text{(VI-16)}$$

For $2 \leq k_B$,

$$\psi = M_o K_e \left(2 k_B - 5 + \frac{10}{3k_B}\right) \qquad \text{(VI-17)}$$

$$\frac{d\Phi}{d\ell} = M_o K_e \left(2 - \frac{6}{k_B} + \frac{5}{k_B^2} - \frac{4}{3k_B^4}\right) \qquad \text{(VI-18)}$$

The normalized work expenditure ψ/p is shown as a function of η for various θ_B in Fig. VI-3. [ψ is expressed as a function of k_B in equations (VI-13 ~ 18) and k_B is a function of η as shown in equations (VI-6 ~ 12).]

Then the energy balance equation (III-6) can be normalized as

$$\bar{p} = 1 + \bar{p}\psi/p, \tag{VI-19}$$

where $\bar{p} = p/\gamma$.

Introducing a normalized thickness of the adherend as

$$\bar{t} = \frac{\sigma_y^2 t}{6E\gamma}, \tag{VI-20}$$

we have the relation

$$\eta = \bar{p}/\bar{t}. \tag{VI-21}$$

Because ψ/p is a function of η, equation (VI-19) gives the relation between $\bar{p}$ and $\bar{t}$. The relation becomes as following, for elastic-perfect plastic adherend;

For $0 \leq k_B < 1$,

$$\bar{p} = 1, \quad \bar{t} = 1/\eta. \tag{VI-22}$$

For $1 \leq k_B \leq 2$,

$\bar{p}\ (\bar{t};\ \theta_B)$ is a solution of

$$\bar{p}^{-3}\ \alpha(1-\alpha)^3 + 2\bar{p}^{-2}\ \alpha(1-\alpha)\ (3\bar{t}-1) + \bar{p}\ \alpha(3\bar{t}-1)^2 - 4\bar{t}^3 = 0 \tag{VI-23}$$

where $\alpha = 1 - \sin\theta_B$. (VI-24)

For $2 < k_B$,

$\bar{p}\ (\bar{t};\ \theta_B)$ is a solution of

$$\bar{p}^{-2}\ (\alpha-1)\ (5\alpha-4) - \bar{p}\ \{3(5\alpha - 4)\ \bar{t} - (9\alpha - 8)\}$$

$$+ 4\ (3\bar{t}^2 - 3\bar{t} + 1) = 0. \tag{VI-25}$$

The $\bar{p}\ (\bar{t};\ \theta_B)$ is shown in Fig. VI-4. As shown in this figure, small change in θ_B changes the behavior of $\bar{p} - \bar{t}$ relation drastically. This indicates that the compliance of substrate plays important role in $\bar{p} - \bar{t}$ relation, because the compliant substrate provides larger value of θ_B. The effect of the substrate compliance is discussed in the following section.

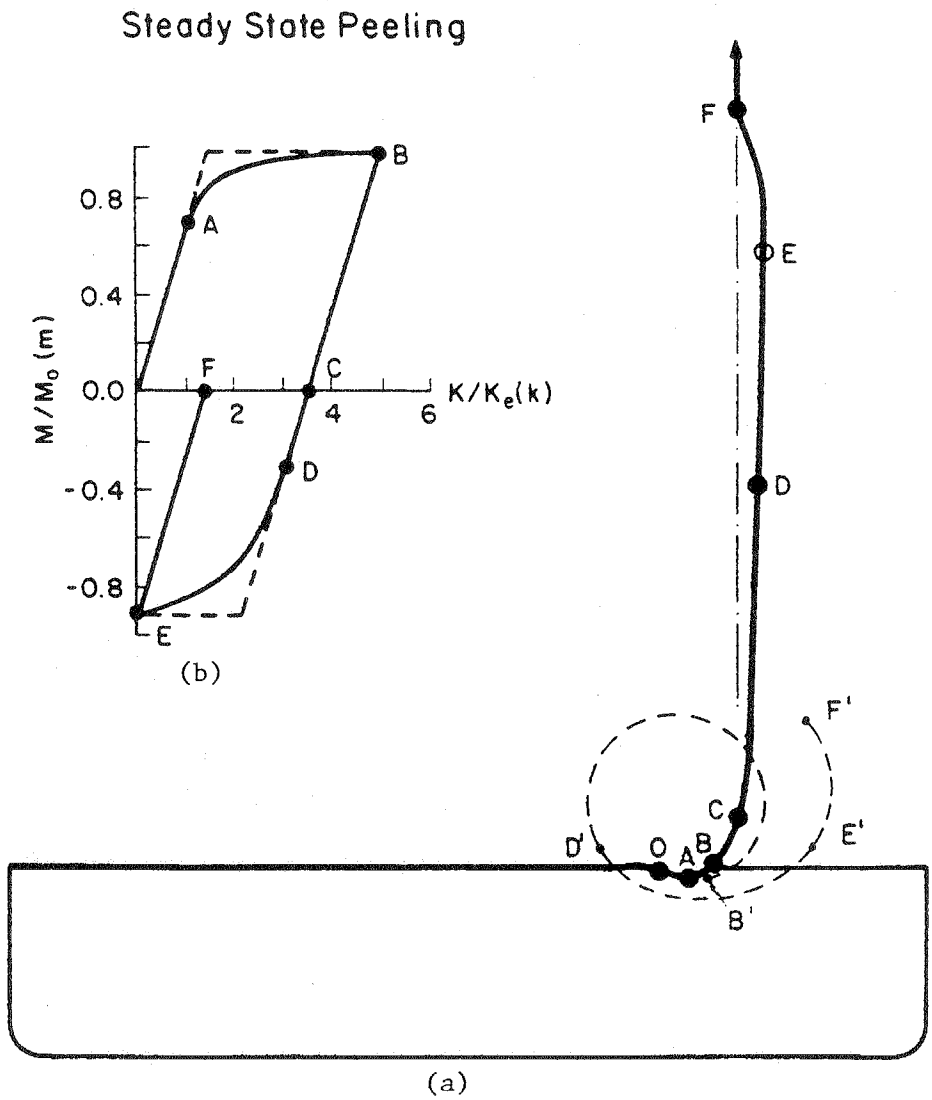
Steady State Peeling
0.8
0.4
0.0
-0.4
-0.8
M/M₀ (m)
2
4
6
K/K_e(k)
A
B
C
D
E
F
(b)
F
E
D
C
B
A
O
D'
E'
F'
B'
(a)

Fig. VI-1

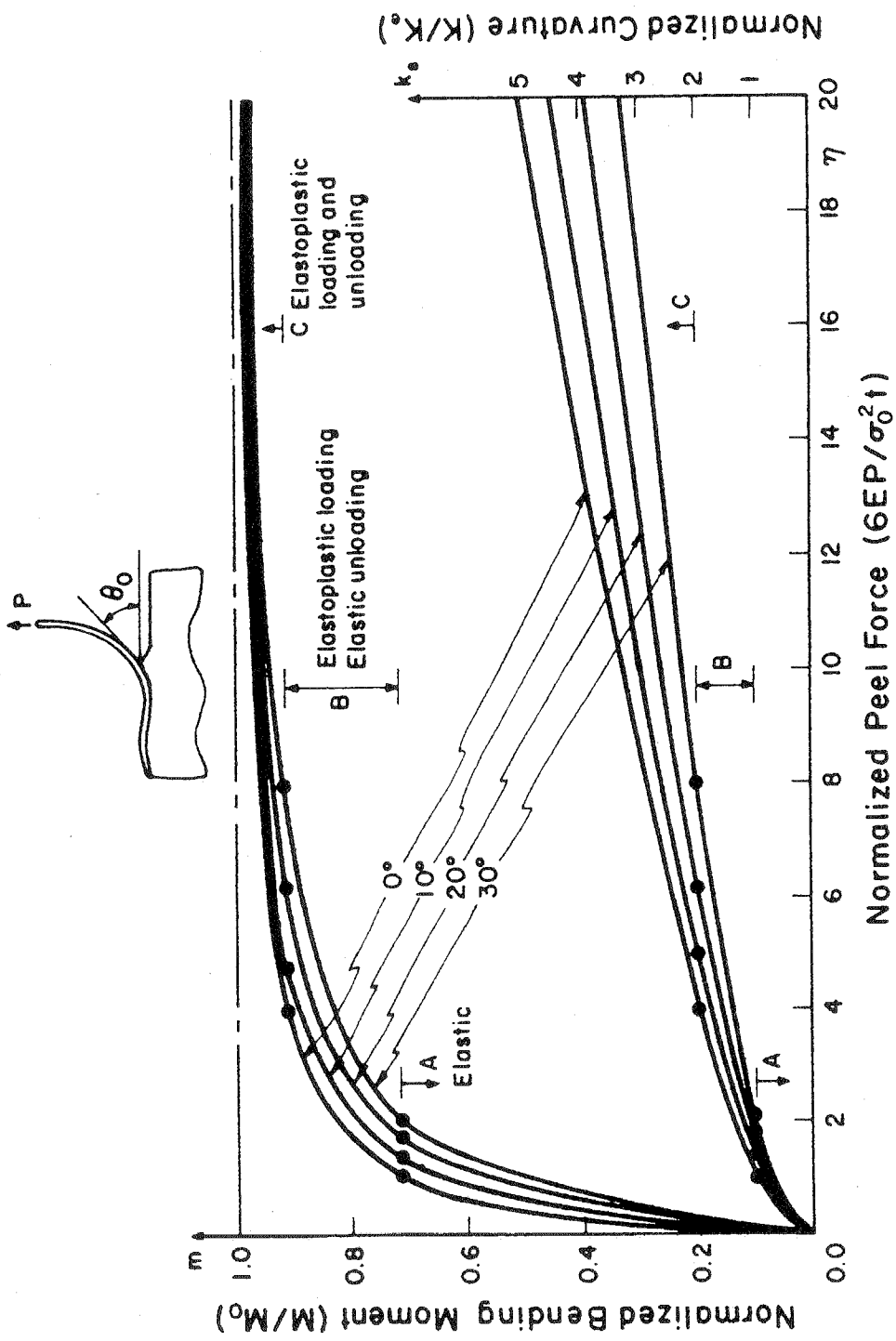
P
θ_o
C Elastoplastic loading and unloading
B Elastoplastic loading Elastic unloading
A Elastic
0°
10°
20°
30°
A
B
C
m
1.0
0.8
0.6
0.4
0.2
0.0
Normalized Bending Moment (M/M_o)
k_s
5
4
3
2
1
2
4
6
8
10
12
14
16
18
20
η
Normalized Peel Force ($6EP/\sigma_o^2 t$)
Normalized Curvature (K/K_o)

Fig. VI-2

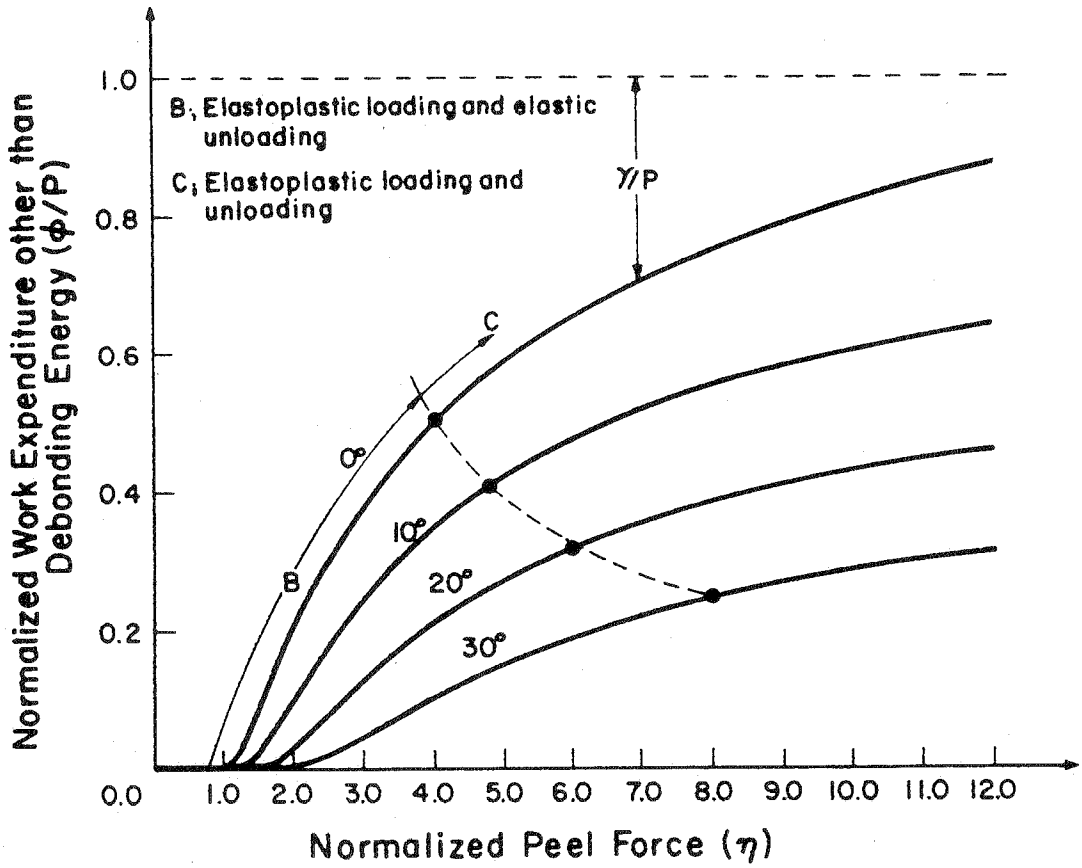
Normalized Work Expenditure other than Debonding Energy (ϕ/P)
1.0
0.8
0.6
0.4
0.2
0.0
B; Elastoplastic loading and elastic unloading
C; Elastoplastic loading and unloading
γ/P
C
B
0°
10°
20°
30°
1.0
2.0
3.0
4.0
5.0
6.0
7.0
8.0
9.0
10.0
11.0
12.0
Normalized Peel Force (η)

Fig. VI-3

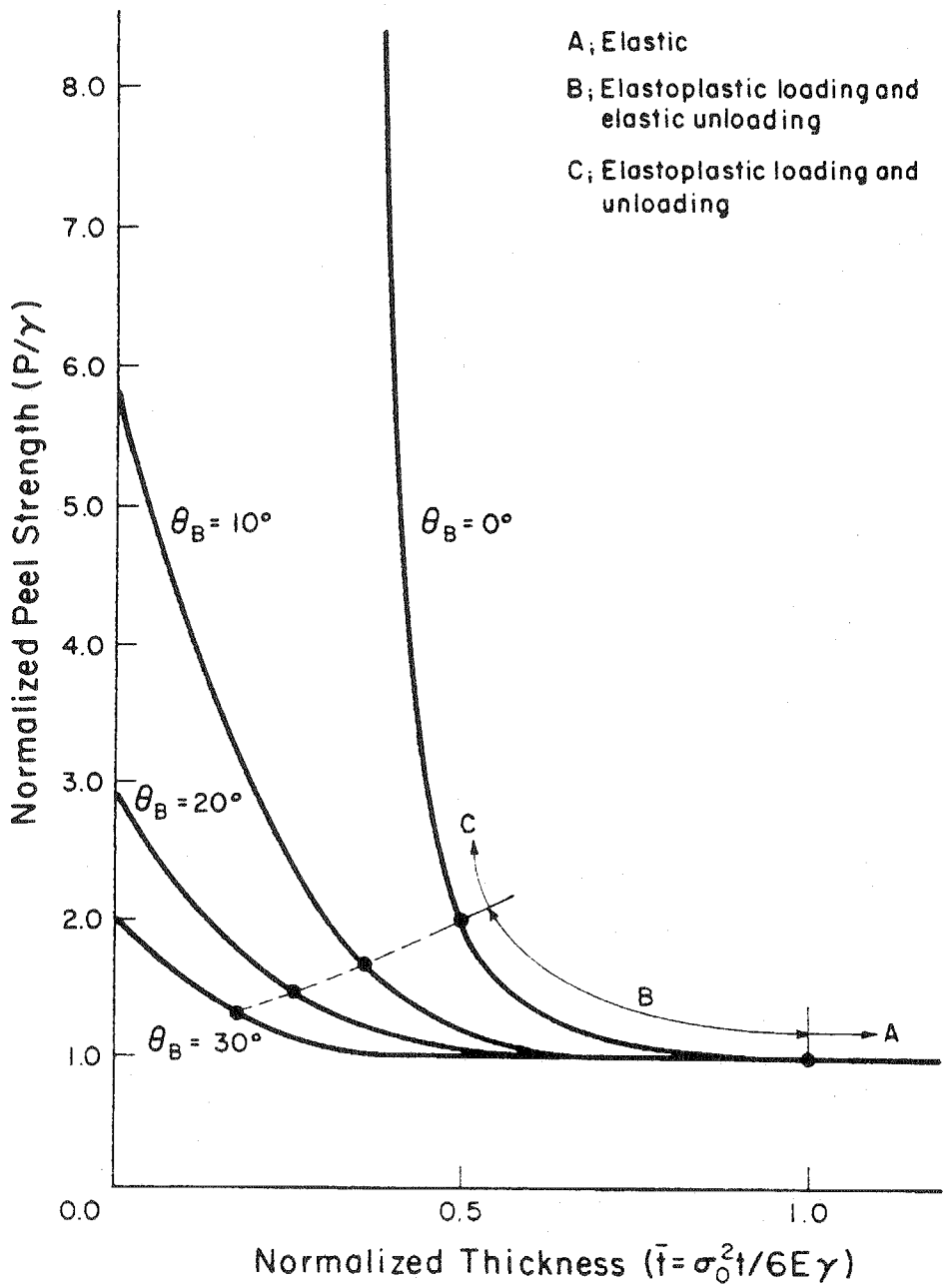
A; Elastic
B; Elastoplastic loading and elastic unloading
C; Elastoplastic loading and unloading
Normalized Peel Strength (P/γ)
8.0
7.0
6.0
5.0
4.0
3.0
2.0
1.0
0.0
0.5
1.0
θB = 10°
θB = 0°
θB = 20°
θB = 30°
C
B
A
Normalized Thickness (t̄ = σ0²t/6Eγ)

Fig. VI-4

VII. Effects of Substrate Properties

In chapter V, it is shown that the substrate remains elastic for thin film peel test. Therefore the elastic compliance of the substrate is the main property of concern in this chapter. As illustrated in chapter VI, the peel force is a strong function of base angle θ_B. The one dimensional model of adherend employed in the energy method has a governing equation that is coupled with the governing equation of substrate deformation only through θ_B. It is clear that θ_B is a function of substrate compliance and the applied moment and force at the root of the adherend. If we neglect the contribution, on θ_B, of plastic bending sector in the bonded section of the adherend, θ_B is a linear function of applied moment and force at the root for linear elastic substrate deformation. In order to see the effects of substrate properties more systematically, a simple Winkler foundation model [24] is employed in this chapter. The schematic of the model is shown in Fig. VII-1. As shown in the figure, the model has 3 sections; (A) elastic beam on elastic foundation, (B) elasto-plastic beam on elastic foundation, (C) free adherend. In principle, various realistic foundation models [25,26,27] can be employed for section (A) and (B).

The governing equation of elastic beam on Winkler foundation is given as

$$\frac{d^4y}{dx^4} + \frac{E_s}{EIh} y = 0 \qquad \text{(VII-1)}$$

where y is the deflection of the beam, E_s is the Young's modulus of the substrate, E is the Young's modulus of adherend, I is the second moment of inertia of the cross section of the adherend, i.e., $t^3/12$, and h is the thickness of the substrate. Then the solution becomes

$$y = e^{-\zeta x} (A \sin \zeta x + B \cos \zeta x) \qquad \text{(VII-2)}$$

where

$$A = - K_e/(2\,\zeta^2) \tag{VII-3}$$

$$B = N/(2\,\zeta^3\,EI) + K_e/(2\,\zeta^2) \tag{VII-4}$$

$$\zeta = \{3\,E_s/(E\,h\,t^3)\}^{1/4} \tag{VII-5}$$

$$\sigma_{int} = E_s\,(\frac{y}{h}) \ . \tag{VII-6}$$

where σ_{int} is the normal stress at the interface. As seen in this solution, the stress (or deflection) distribution has a wave length of $2\pi/\zeta$. Also it can be seen that for $x = 2\pi/\zeta$ the amplitude decays to the value less than 0.2% of the maximum normal stress.

For the elasto-plastic bending part, the governing equation becomes

$$\frac{d^2M(K)}{ds^2} - KT + \frac{E_s}{h}\,y = 0 \ . \tag{VII-7}$$

However, this equation is nonlinear and the boundary of the elasto-plastic part is not known in a priori, so that some ad hoc approximation has to be considered, retaining physical significance in the approximation. Because the length, s_o, of the elasto-plastic part is only order of the thickness of the adherend, the variation of the curvature is assumed linear along the length of the adherend. Then,

$$K = (K_B - K_e)\,(s/s_o) + K_e \tag{VII-8}$$

and, because $K = \frac{d\theta}{ds}$, θ_B becomes

$$\theta_B = \theta_E + \frac{1}{2}\,(K_B + K_e)\,s_o \ . \tag{VII-9}$$

Since $K \ \frac{d^2y}{ds^2}$, equation (VII-8) is integrated twice and the integration constants and s_o are determined by the force balance, moment balance of the

section s_o and the patching conditions at the boundaries. The patching conditions are, the continuities of displacement, slope, and moment of the adherend at the boundaries. Then, nondimensionalizing s_o as $z_o = \zeta s_o$, we can get

$$k_B = C_1 (Z_o) + C_2 (Z_o) (\eta/\bar{n}) \tag{VII-10}$$

where $\bar{n} = \zeta/K_e$ is a nondimensionalized relative stiffness of the substrate and

$$c_1(z_o) = (-33 z_o^6 - 99 z_o^5 + 363 z_o^4 + 120 z_o^3 + 180 z_o + 90)/c_3(z_o) \tag{VII-11}$$

$$c_2(z_o) = (-30 z_o^5) + 30 z_o^4 + 75 z_o^3 - 45 z_o^2 - 45 z_o)/c_3(z_o) \tag{VII-12}$$

$$c_3(z_o) = 22 z_o^6 - 9 z_o^5 - 12 z_o^4 - 90 z_o^2 + 180 z_o + 90. \tag{VII-13}$$

where z_o is a solution of

$$6 \{c_1(z_o) + c_2(z_o) (\eta/\bar{n})\}^2 - \{c_1(z_o) + c_2(z_o) (\eta/\bar{n})\} \times$$
$$[12 - \eta \sin\{B_1(z_o)/\bar{n} + \eta B_2(z_o)/\bar{n}^2\} + \eta] + 8 = 0, \tag{VII-14}$$

$$B_1(z_o) = \bar{n} \{A_1(z_o) c_1(z_o) + A_2(z_o)\}, \tag{VII-15}$$

$$B_2(z_o) = \bar{n} A_1(z_o) c_2(z_o), \tag{VII-16}$$

$$A_1(z_o) = z_o(6-7 z_o^2 + 12 z_o)/\{12 \bar{n}(1 - z_o^2 + 2 z_o)\} \tag{VII-17}$$

$$A_2(z_o) = \eta/(4\bar{n}^2) + z_o/(2\bar{n}) + 1/n - \{\bar{n} z_o^3 - (4\bar{n} + \eta) z_o^2$$
$$+ (4\bar{n} + 2\eta) z_o\}/\{4\bar{n}^2 (1 - z_o^2 + 2 z_o)\}. \tag{VII-18}$$

Then, θ_B becomes

$$\theta_B = A_1(z_o) k_B + A_2(z_o). \tag{VII-19}$$

Employing this result in equations (VI-6,8,10) the $\bar{p} - \bar{t}$ relation is obtained. The relation is plotted in Fig. VII-2 for $\bar{n}$ = 10 and 20. As shown in this figure. Compliant (smaller $\bar{n}$) substrate reduces the peel value substantially and shows the trends observed in experiments - the peel value has a peak at a certain thickness of the adherend. In chapter VI and VII, we have introduced the analytic method to get $\bar{p} - \bar{t}$ relationship for elastic and perfectly plastic adherend on an elastic substrate. For general constitutive relations, the procedure of obtaining $\bar{p} - \bar{t}$ relationship is indentical to the procedure discussed in these two chapters; only need more laborious calculations. In the following chapter (VIII), the use of $\bar{p} - \bar{t}$ relation as a universal peel diagram will be discussed. Fig. VII-3 shows the comparison between the theoretical prediction and the experimental measurements. The theoretical prediction is based on 2-parameter power law isotropic hardening of adherend. As an approximation procedure, the results of chapter VI, equations (VI-22 - 25) is used by adjusting the effective yield stress to account the hardening. The adjustment was made in a iterative procedure to satisfy the following condition.

$$\int_0^{\varepsilon_{max}} \sigma \, d\varepsilon = \sigma_o \, \varepsilon_{max} - \sigma_o^2/E \qquad \text{(VII-20)}$$

where $\varepsilon_{max} = K_B t/2$.

The prediction remarkably matches the experimental values. Also the extraction of adhesion energy from the peel values was made by $\gamma = p/\bar{p}$. A simple prediction of γ by choosing the effective yield stress as $(\sigma_u + \sigma_y)/2$ for elastic perfect plastic model gives increasing values as the thickness, as shown in Fig. VII-4. However, when the hardening and the substrate compliance were properly accounted, the adhesion energy turns out to be constant

regardless of the thickness of the adherend.

Throughout the analysis, it is shown systematically that the yield stress, hardening coefficient of the adherend and the substrate compliance, play important roles in determining the adhesion energy from the peel strength.

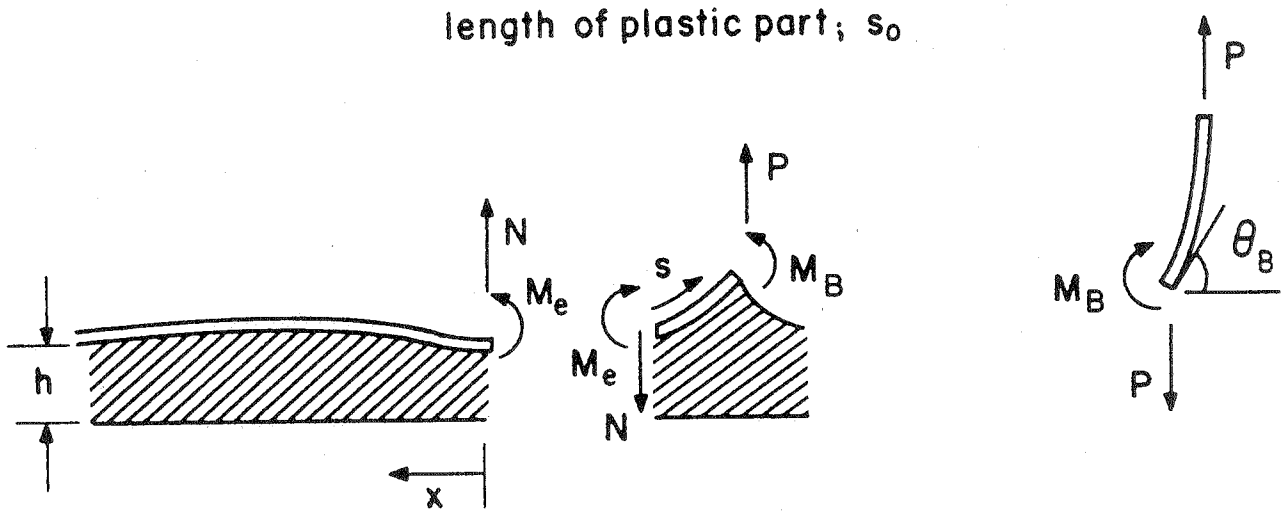

Fig. VII-1

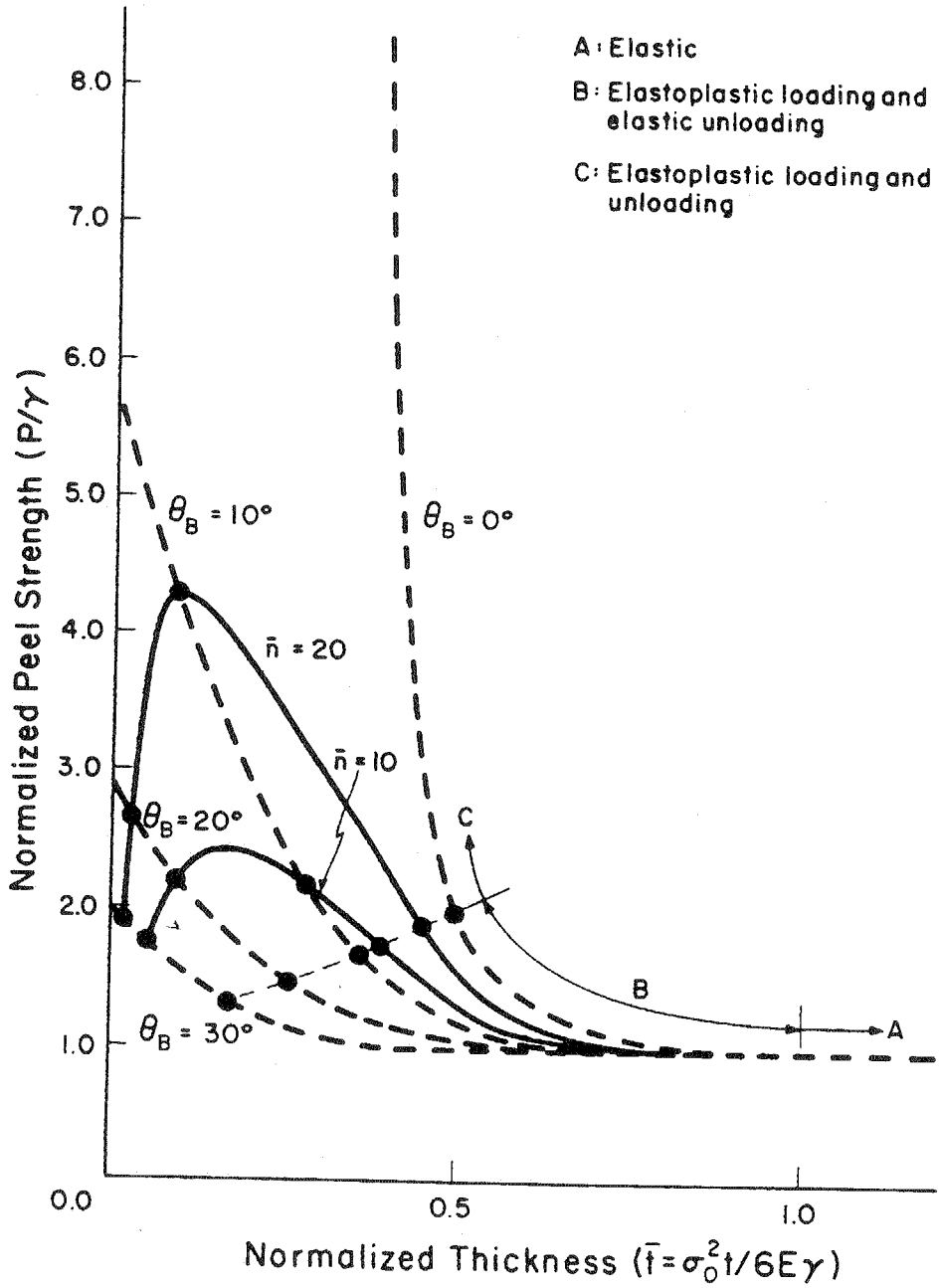
A: Elastic
B: Elastoplastic loading and elastic unloading
C: Elastoplastic loading and unloading
8.0
7.0
6.0
5.0
4.0
3.0
2.0
1.0
0.0
0.5
1.0
Normalized Peel Strength (P/γ)
Normalized Thickness ($\bar{t}=\sigma_0^2 t/6E\gamma$)
θ_B = 10°
θ_B = 0°
θ_B = 20°
θ_B = 30°
$\bar{n}$ = 20
$\bar{n}$ = 10
A
B
C

Fig. VII-2

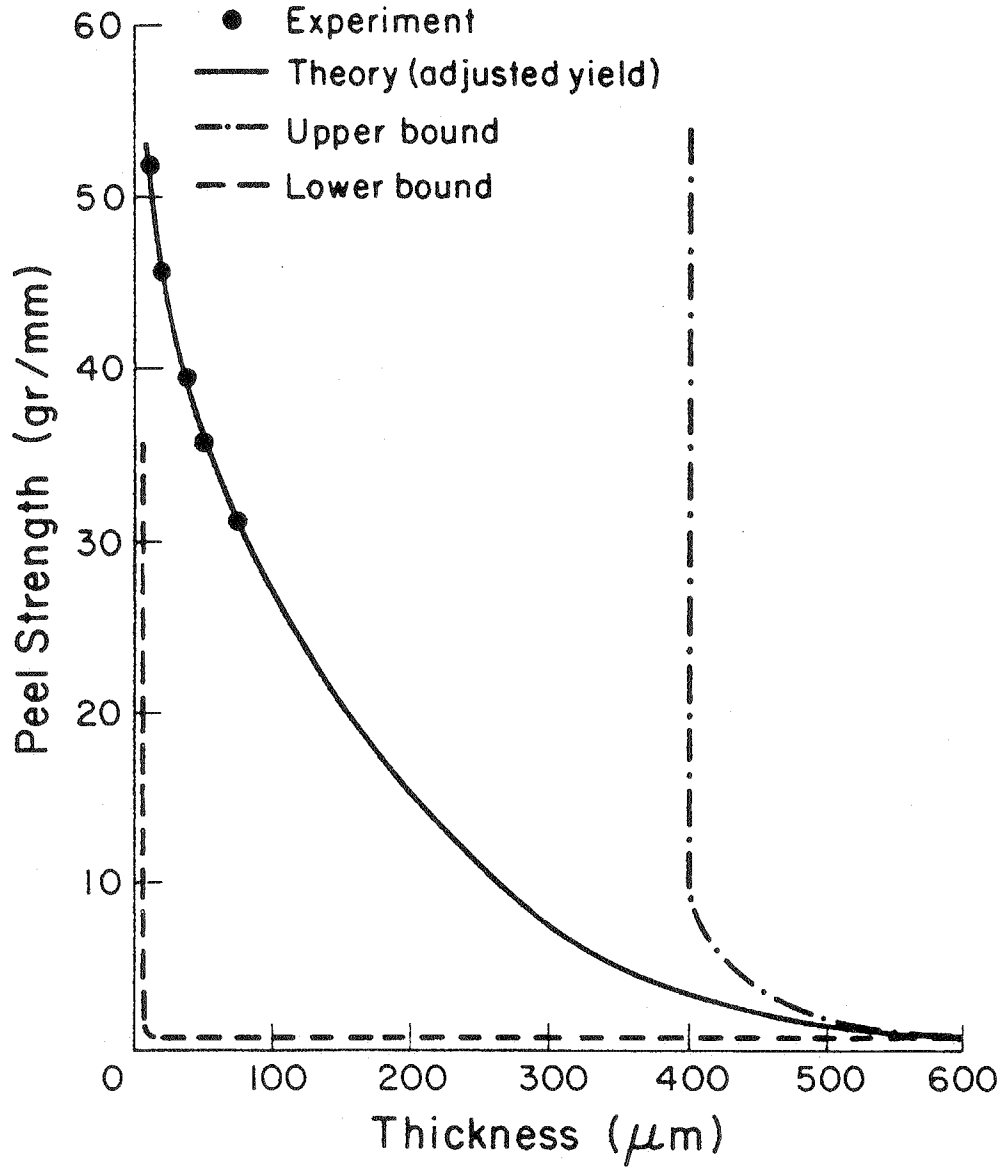
Experiment
Theory (adjusted yield)
Upper bound
Lower bound
Peel Strength (gr/mm)
60
50
40
30
20
10
0
100
200
300
400
500
600
Thickness (μm)

Fig. VII-3

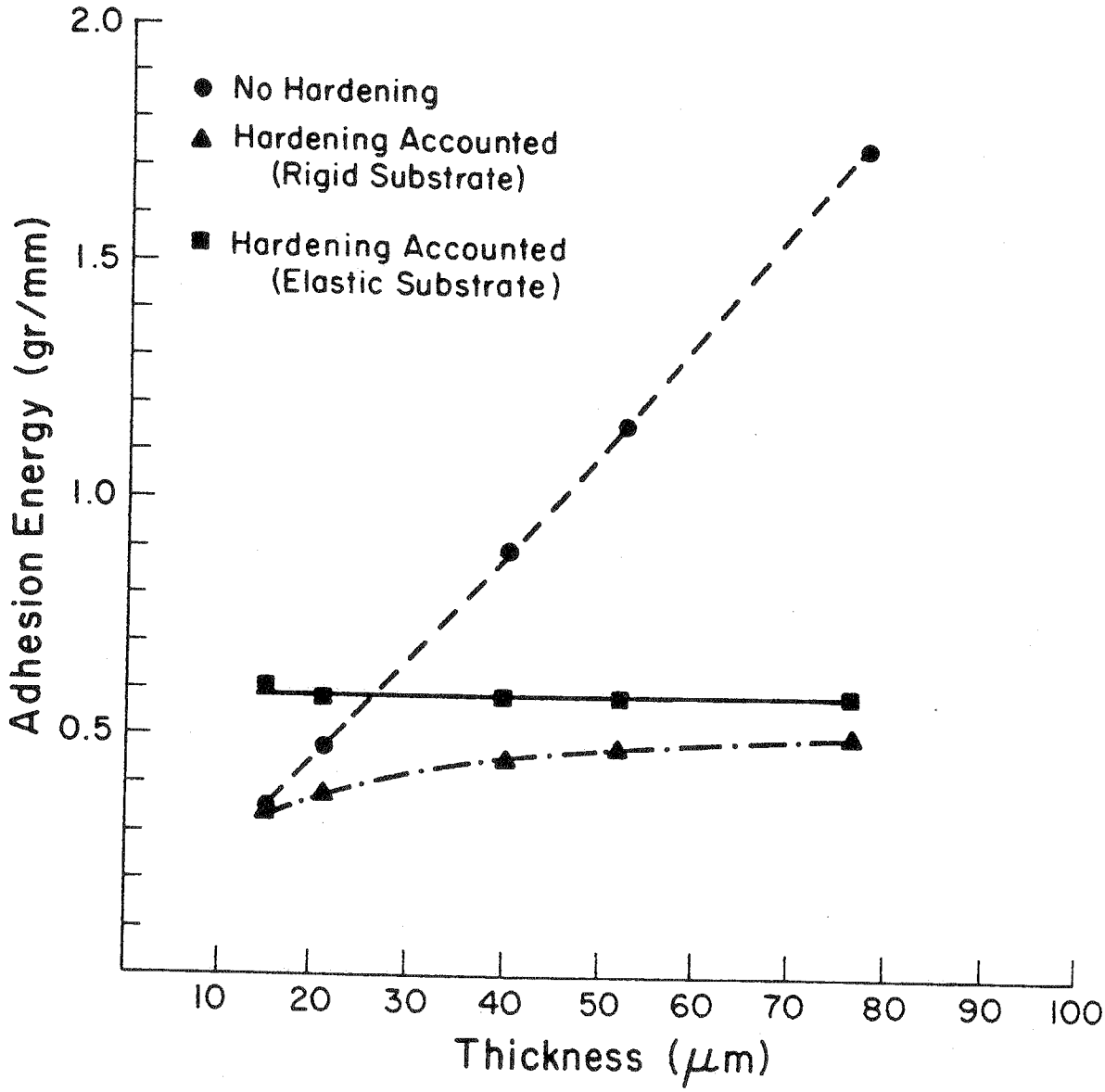
2.0
1.5
1.0
0.5
Adhesion Energy (gr/mm)
No Hardening
Hardening Accounted
(Rigid Substrate)
Hardening Accounted
(Elastic Substrate)
10
20
30
40
50
60
70
80
90
100
Thickness (μm)

Fig. VII-4

VIII. Universal Peel Diagram

In this chapter, the inter-relation among the peel strength, p, and the adhesion energy, γ , and the thickness, t, is expressed as a diagram. The diagram is, of course, dependent upon various combinations of bulk properties E, σ_y, n, s of the adherend and the compliance of the substrate. Assuming either isotropic or kinematic hardening behavior of the adherend, the peel strength can be expressed as a functional form as,

$$p = f(\gamma, t, \sigma_y, E, E_s, n, s, \nu, \nu_s), \tag{VIII-1}$$

where ν and ν_s represent the Poisson's ratio of the adherend and the substrate respectively. n and s are hardening coefficients defined in equation (IV-20). Then the fundamental relation can be reduced by a dimensional analysis as

$$p/\gamma = g(\sigma_y^2\, t/6\, E\gamma,\ E_s/E,\ n,\ s,\ \nu,\ \nu_s). \tag{VIII-2}$$

Therefore, for a given system of the adherend and substrate, the functional relation becomes

$$\bar{p} = g^*\ (\bar{t};\ E_s/E,\ n,\ s,\ \nu,\ \nu_s), \tag{VIII-3}$$

where E_s/E, n, s, ν, ν_s are all constant. This indicates that there is a simple and unique functional relationship between $\bar{p}$ and $\bar{t}$ for the given system. The relationship, $\bar{p} - \bar{t}$, expressed on a log-log scale is going to be called "Universal Peel Diagram of the System." The analytic method of obtaining $\bar{p} - \bar{t}$ relation has been already discussed in chapter VI and VII. On the peel diagram, a diagonal axis represents η-axis as shown in Fig. (VIII-1), because

$$\log \bar{p} = \log \bar{t} + \log \eta \qquad \text{(VIII-4)}$$

from equation (VI-21). Therefore, if you get η from a peel test data, the cross-section point of η = constant and the universal curve represents the state of adhesion on the diagram. Reading $\bar{p}$ of the point on the vertical axis, we can get γ readily. Similarly, if we know the thickness $\bar{t}$, we can read $\bar{p}$ or visa versa. The universal peel diagram can be constructed purely by peel test experiment. Carrying out the peel test with various thickness of the adherend for a same but unknown adhesion energy, we can plot $\bar{p} - \bar{t}$ with arbitrary constant value of γ for the test data. Then, by translating the group of the data points along η = constant lines on the diagram, we can construct the universal curve of the system.

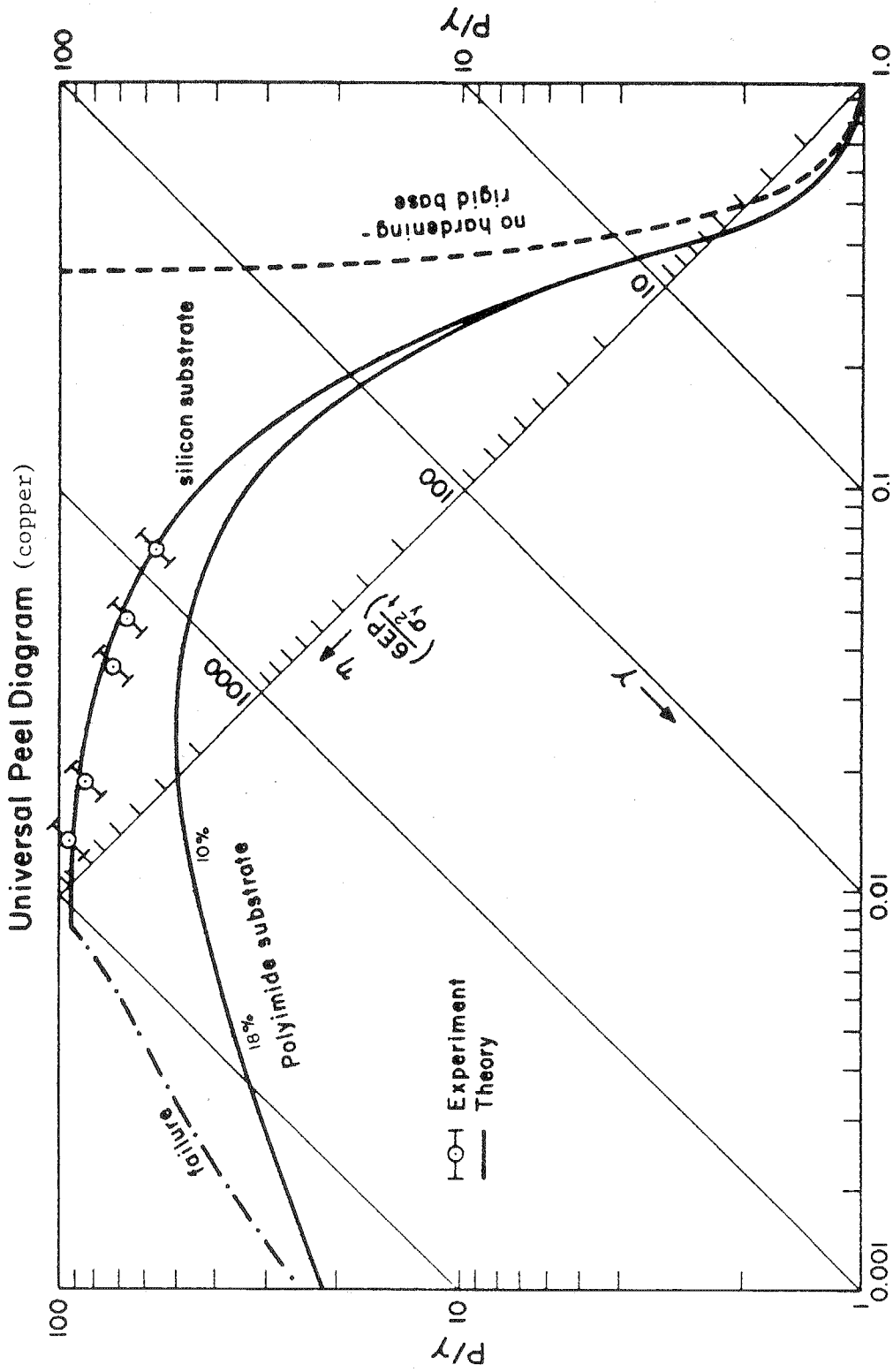
Universal Peel Diagram (copper)
P/γ
100
10
1
1.0
0.1
0.01
0.001
$\bar{t}, (\sigma_y^2 t/6E\gamma)$
γ
$\gamma\left(\frac{6}{E}\left|\frac{\sigma_y^2}{\beta}\right|^2 t\right)$
10
100
1000
no hardening - rigid base
silicon substrate
10%
18%
Polyimide substrate
failure
Experiment
Theory

Fig. VIII-1

IX. Relations Between Peel, Pull and Fracture Tests. (Conversion methods).

In the computer industries, the pull test is also widely used to calibrate the state of adhesion. A schematic of the pull test is shown in Fig. IX-1. Pull test is carried out by pulling a pin braized or epoxy-bonded to a thin film disk that is attached to a substrate. Then the pull strength is defined as the average stress of pulling at the interface at onset of failure. Although this test gives certain measure of adhesion state, test values are so much sensitive to loading alignment and microflaws that test data scatters widely. However, provided the loading is satisfactorily aligned and the diameter of the disk is very small (order of 1 ~ 2 mm), let's assume that the debonding process is similar to the process at peeling crack front. Then if the microflaw size (order of tens ~ hundreds of Angstrom) is much smaller than the thickness of the film and is distributed randomly, we can consider an effective debonding distance δ_t, which is analogous to the crack tip opening displacement of a steadily moving crack. Then from equation (III-5)

$$\overline{\sigma}_{bs} = \frac{\gamma}{\delta_t} . \qquad \text{(IX-1)}$$

The average bond strength at the interface can be considered as the pull strength. δ_t is constant for an interface of given combination of materials, unless there is a relatively large flaw. For example, peel test and the result of finite element analysis predict $\delta_t = 0.089$ μm for copper and polyimide joint. This δ_t is estimated by $\delta_t = \frac{\gamma}{(\sigma_{tip}^2 + \tau_{tip}^2)^{1/2}}$, because there is mixed-mode loading at the crack tip. Therefore δ_t is the magnitude of vectorial crack-opening-displacement. One set of pull test data provided by Dr. L. Lee and T. Wray of Endicott IBM gives $\delta_t = 0.119$ μm for the copper-polyimide joint. This is based on the average value of a set of pull test

values of the same adhesion. Assuming δ_t (- 0.119 μm) is the system constant, peel-pull relation is predicted, for a given thickness (88 μm) of the adherend, from equation (IX-1),

$$\sigma_{bs} = \frac{\gamma(p,t;\ \sigma_y,E,E_s,n,s,\nu,\nu_s)}{\delta_t} \qquad \text{(IX-2)}$$

Because γ-p-t relation is given in the universal peel diagram, we can predict $\bar{\sigma}_{bs}$ from the peel value through equation (IX-2). The prediction is shown in Fig. IX-2 and it agrees well with experimental observations. It is believed that if δ_t obtained from peel test and FEM result is used, the predicted pull strength will be an upper bound of observed pull values. This is because of the effect of misalignment, flaws and stress concentration in pull test. If there is a substantially large flaw of diameter 'a_f' in the interface the pull strength will be governed by the flaw and it will become

$$\sigma = \left\{\frac{\gamma\ E_{eff}}{a_f}\right\}^{1/2}$$

where E_{eff} is an effective modulus of the bimaterial system. The method of stress analysis for pull configuration is well discussed in References [28,29,30].

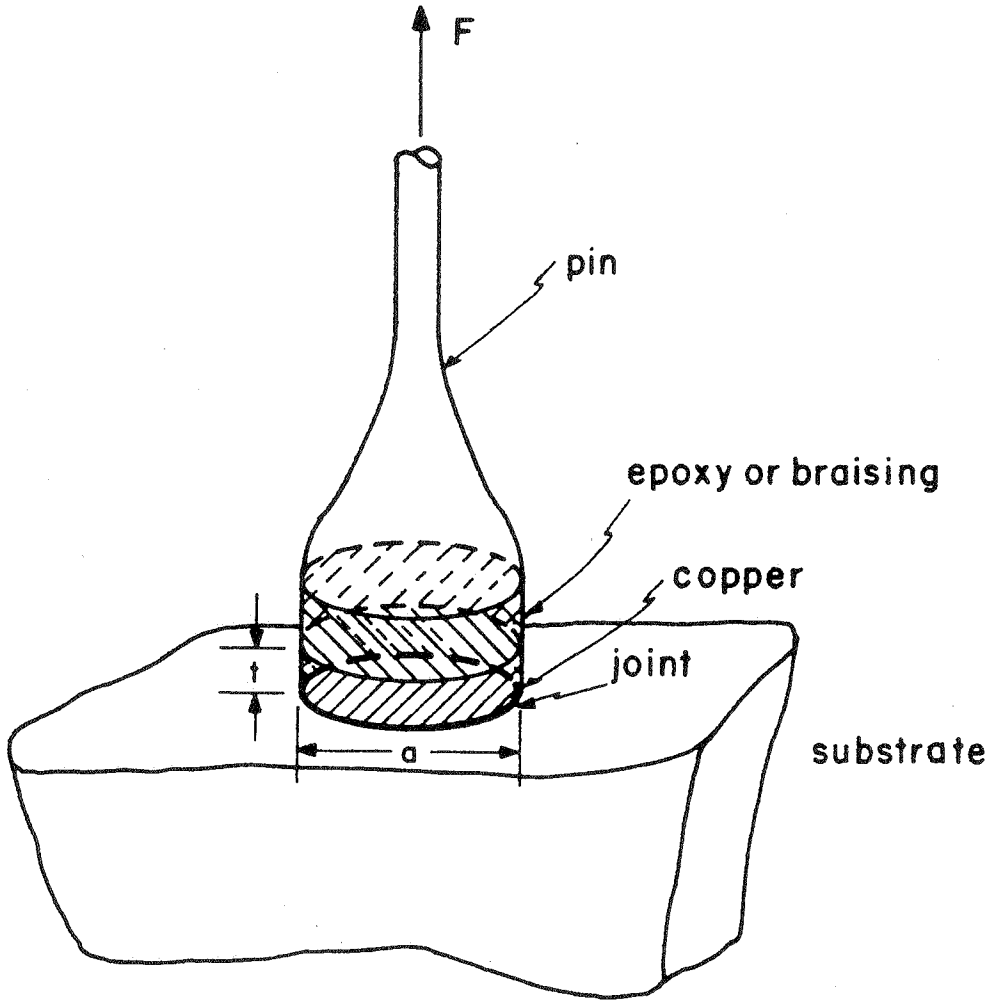

Pull Test

Fig. IX-1

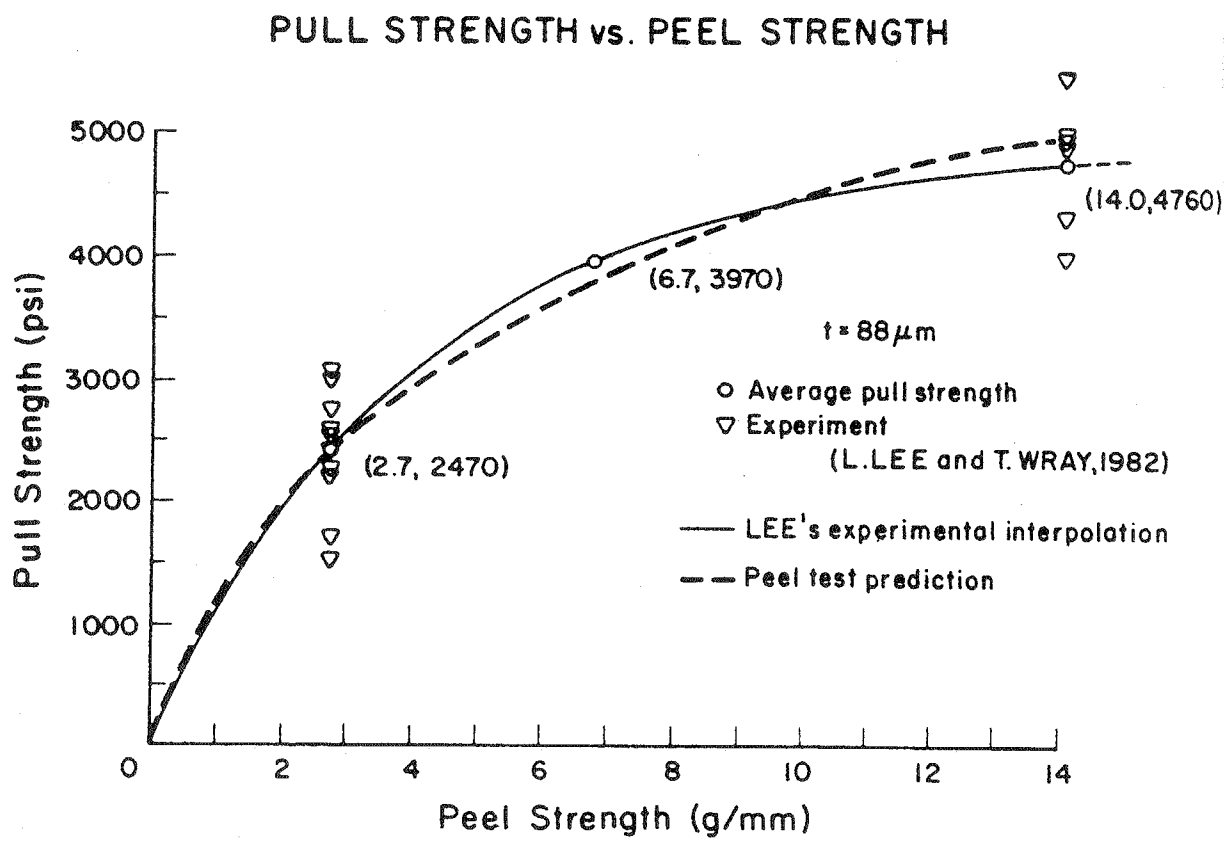
PULL STRENGTH vs. PEEL STRENGTH
Pull Strength (psi)
5000
4000
3000
2000
1000
0
2
4
6
8
10
12
14
Peel Strength (g/mm)
(14.0,4760)
(6.7, 3970)
(2.7, 2470)
t = 88μm
Average pull strength
Experiment
(L.LEE and T.WRAY,1982)
LEE's experimental interpolation
Peel test prediction

Fig. IX-2

X. Conclusion

In this report, energy balance concept has been employed to extract the adhesion energy of thin metalic film joint. Mode of deformation at onset of crack propagation has been analyzed by an approximation method and finite element method. These analysis give information on adherend-deformation and stress-distribution at interface at the loading stage. The analysis was extended for steady state peel propagation. In this analysis the adhesion energy could be extracted from peel strength. The peel strength and adhesion energy relation is strongly dependent upon the bulk properties of the adherend and substrate. It is strongly dependent upon the thickness of the adherend. These inter-relations could be figured out by the analysis, and it is expressed as a universal peel diagram. Through the use of this universal peel diagram, we can get the adhesion energy readily from the peel strength and the adhesion energy plays the central role to bridge the pull and peel test values. This report gives the skeleton of the analysis of peel and pull tests. Beyond this, we need the analysis of more sophisticated and realistic situations, such as the effect of residual stress, peeling rate, contamination and imperfection at the interface.

Acknowledgement

Support of Drs. C. K. Lim, L. Lee, P. Geldermans, R. Lacomb, J. Hurst and J. Kim are greatly appreciated. The numerical computations in Chapter V was carried out by Dr. N. Aravas while he was a graduate assistant at the University of Illinois at Urbana-Champaign. He is currently working at Hibbitt, Karlsson and Sorenson, Inc., Providence, R.I. His assistance is gratefully acknowledged. Also valuable discussions and encouragement of Professor R. T. Shield is gratefully acknowledged.

References

1. Spies, G. J., "The Peel Test on Redux-bonded Joints," Aircraft Engineering, 25, 1953, pp 64-70.

2. Kaelble, D. H., "Theory and Analysis of Peel Adhesion: Bond Stresses and Distributions," Trans. Society of Rheology, 4, 1960, pp 45-73.

3. Yurenka, S., "Peel Testing of Adhesive Bonded Metal," Jn. Appl. Polymer Sci., 6, 1962, p 136.

4. Duke, A. J. and Stanbridge, R. P., "Cleavage Behavior of Bonds Made with Adherends Capable of Plastic Yield," Jn. Appl. Polymer Sci., 12, 1968, pp 1487-1503.

5. Crocombe, A. D. and Adams, R. D., "An Elasto-plastic Investigation of the Peel Test," Jn. Adhesion, 13, 1982, pp 13-241.

6. Gent, A. N. and Hamed, G. R., "Peel Mechanics for an Elasto-plastic Adherend," Jn. of Appl. Polymer Sci., 21, 1977, pp 2817-2831.

7. Kim, K. S., "Elasto-plastic Analysis of Peeling," Jn. Adhesion (in preparation) 1985.

8. Prager, W., "A new method of analyzing stresses and strains in work hardening solids," Jn. of Appl. Mechanics, 23, 1956, pp 493-496.

9. Prager, W., "Strain hardening under combined stress," Jn. of Appl. Physics, 16, 1945, pp 837-840.

10. Wells, A. A., "Unstable Crack Propagation in Metals: Cleavage and Fast Fracture," Symp. Crack Propagation, Cranfield, 1961.

11. Sih, G. C., "A Special Theory of Crack Propagation," Mechanics of Fracture, ed. G. C. Sih, Noordhoff Inc. Publishing, Leyden, 1973, pp 21-45.

12. Rice, J. R., "A Path Independent Integral and the Approximate Analysis of Strain Concentration by Notches and Cracks," Jn. of Appl. Mechanics, 35, 1963, pp 379-386.

13. Love, A.E.H., A Treatise on the Mathematical Theory of Elasticity, Dover Publications, Inc. N.Y. 1944.

14. Hill, H., The Mathematical Theory of Plasticity, Oxford University Press, 1950.

15. Hodge, P. G., Plastic Analysis of Structures, McGraw-Hill, 1959.

16. Bisshopp, K. E. and Drucker, D. C., "Large Deflection of Cantilever Beams," Quarterly of Applied Mathematics, Vol. 3, pp 272-275 (1945).

17. Rice, J. R. and Tracey, D. M., Journal of the Mechanics and Physics of Solids, 17, 1969, pp 201-217.

18. Hibbitt, Karlsson and Sorenson, ABAQUS Manual - Theory, 1984.

19. Hibbitt, Karlsson and Sorenson, ABAQUS Manual - Users, 1984.

20. Nagtegal, J. C., Parks, D. M. and Rice, J. R., Computer Methods in Applied Mechanics and Engineering, 4, 1974, pp 153-177.

21. Liechti, K. M., "The Application of Optical Interferometry to Time Dependent Unbonding," Ph.D. Thesis, Caltech, Pasadena, CA 1980.

22. Chen, W. T. and Flavin, T. F., "Mechanics of Film Adhesion: Elastic and Elastic-plastic Behavior," IBM Jn. of Research and Development, 16, 1972, pp. 203-213.

23. Drugan, W. J., Rice, J. R. and Sham, T. L., "Asymptotic Analysis of Growing Plane Strain Tensile Cracks in Elastic-Ideally Plastic Solids," Jn. Mech. Phys. Solids, 30, 1982, pp 447-473.

24. Winkler, E., Die Lehre van der Elastizität und Festigkeit. Prag: Dominicas, 1867, 99.

25. Reissner, E., "A note on deflections of plates on a viscoelastic foundation," Jn. Appl. Mech., 25, 1958, pp 144-145.

26. Hetenyi, M., "Beams and plates on elastic foundations and related problems," Applied Mechanics Reviews, 19, 1964, pp 95-102.

27. Kerr, A. D., "A study of a new foundation model," Acta Mechanica, 1, 1965, pp 135-147.

28. Lee, L. and Wray, T., IBM internal report, and private communication, 1982.

29. Shield, R. T., "The Application of Limit Analysis to the Determination of the Strength of Butt Joints," Quarterly of Applied Mathematics, 15, 1957, pp. 139-147.

30. Sneddon, I. N., "The distribution of stress in adhesive joints," Adhesion, Ed. by Eley, D. D., Oxford University Press, 1961, pp. 207-253.